ACS OMEGA

Open Access

http://pubs.acs.org/journal/acsodf

Article

Crystal Structure, Hirshfeld Surface Analysis, and Biological Activities of Schiff-Base Derivatives of 4-Aminoantipyrine

Esteban Aguilar-Llanos, Saskya E. Carrera-Pacheco, Rebeca González-Pastor, Johana Zúñiga-Miranda, Cristina Rodríguez-Pólit, Arianna Mayorga-Ramos, Oscar Carrillo-Naranjo, Linda P. Guamán, Juan Carlos Romero-Benavides, Carlos Cevallos-Morillo, Gustavo A. Echeverría, Oscar E. Piro, Christian D. Alcívar-León, and Jorge Heredia-Moya*

Cite This: *ACS Omega* 2023, 8, 42632−42646

Read Online

ACCESS | Metrics & More | Article Recommendations | Supporting Information

ABSTRACT: Eight Schiff bases, synthesized by the reaction of 4-aminoantipyrine with different cinnamaldehydes, were studied in the solid state by using vibrational spectroscopy (IR) and X-ray diffraction techniques. The analysis was extended to the solution phase through ultraviolet−vis, fluorescence spectroscopy, and cyclic voltammetry. Finally, the crystal structures of four compounds (**3b**, **3d**, **3g**, and **3h**) were determined and studied. In addition to the experimental study, theoretical calculations using the semiempirical method PM6/ZDO were performed to understand better the compound's molecular properties, UV−vis, and infrared spectra. The primary difference is the angular conformation of the terminal phenyl rings around the corresponding linking C−N and C−C σ-bonds. Furthermore, as a result of extended bonding, the > C═N− azomethine group-containing C_{pyr}−N═(CH)−(CR)═(CH)−C_{bz} chain (with R═H for **3b**, **3d**, and **3h**, and R═CH_3 for **3g**) is planar, nearly coplanar, with the mean plane of the pyrazole ring. Hirshfeld surface (HS) analysis was used to investigate the crystal packing and intermolecular interactions, which revealed that intermolecular C−H···O and C−H···N hydrogen bonds, $\pi\cdots\pi$ stacking, and C−H···π and C═O···π interactions stabilize the compounds. The energy contributions to the lattice energies of potential hydrogen bonds were primarily dispersive and repulsive. All derivatives were tested *in vitro* on LPS-stimulated mouse macrophages to assess their ability to suppress the LPS-induced inflammatory responses. Only a slight reduction in the level of NO production was found in activated macrophages treated with **3h**. Additionally, the derivatives were tested for antimicrobial activity against several clinical bacteria and fungi strains, including three biofilm-forming microorganisms. Nevertheless, only Schiff base **3f** showed interesting antibacterial activities with minimum inhibitory concentration (MIC) values as low as 15.6 μM against *Enterobacter gergoviae*. On the other hand, Schiff base **3f** and, to a lesser extent, **3b** and **3h** showed antifungal activity against clinical isolates of *Candida*. The lowest MIC value was for **3f** against *Candida albicans* (15.6 μM). It is interesting to note that the same Schiff bases exhibit the highest activity in both biological evaluations.

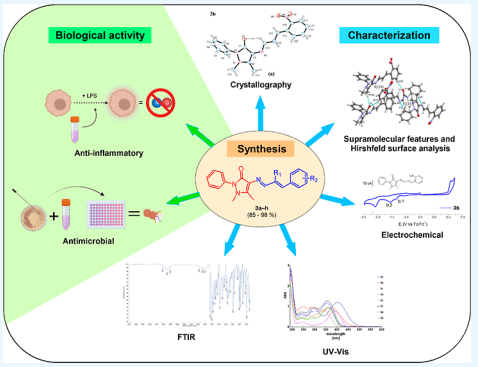

INTRODUCTION

Schiff base derivatives of 4-aminoantipyrine (4-AAP) are an intriguing class of organic compounds with a five-membered ring containing two nitrogen atoms, a double bond, an imine, and a carbonyl group.[1] They are easily synthesized by condensing the amine group in 4-AAP with the carbonyl group attached to different aldehydes or ketones, facilitating access to a broad range of compounds with high yields. Additionally, the electron-donating nitrogen in the imine bond generates L-type ligands, capable of forming complexes with nearly any metal;[2−4] therefore, these compounds have been employed successfully in a variety of applications, including optical[5] and nonlinear optical applications,[6,7] analytical,[8] sensor development,[9] solar cells,[10] catalysis,[11] corrosion inhibitors,[12] organic synthesis intermediates, new drug development,[13,14] and more.

A wide range of biological activities, including anti-leishmanial, analgesic, anti-inflammatory, anticancer, and antiviral activities, has been reported for Schiff bases.[15,16] They also have strong radical scavenging and AChE enzyme inhibition activity,[17−20] as well as antibacterial and antifungal activities against several pathogens.[21,22] The mechanism of action of 4-AAP compounds is thought to involve their ability to interact with biological macromolecules such as proteins[23,24]

Received: July 24, 2023
Accepted: September 26, 2023
Published: October 31, 2023

Scheme 1. Synthesis of Schiff Base Derivatives 3a−h

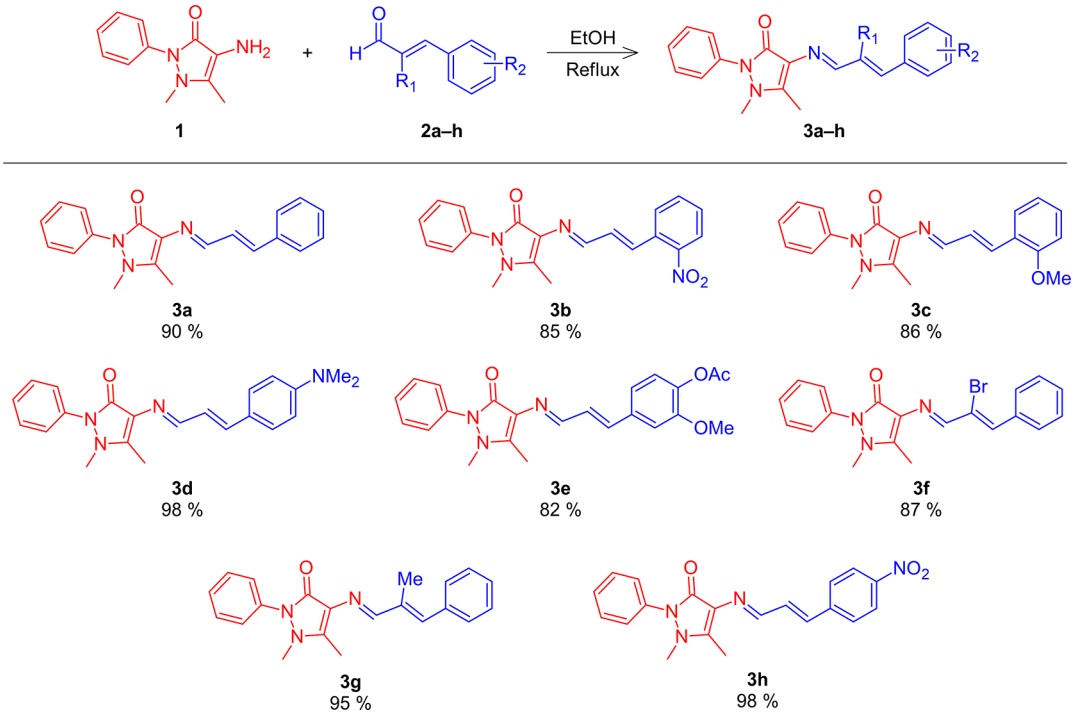

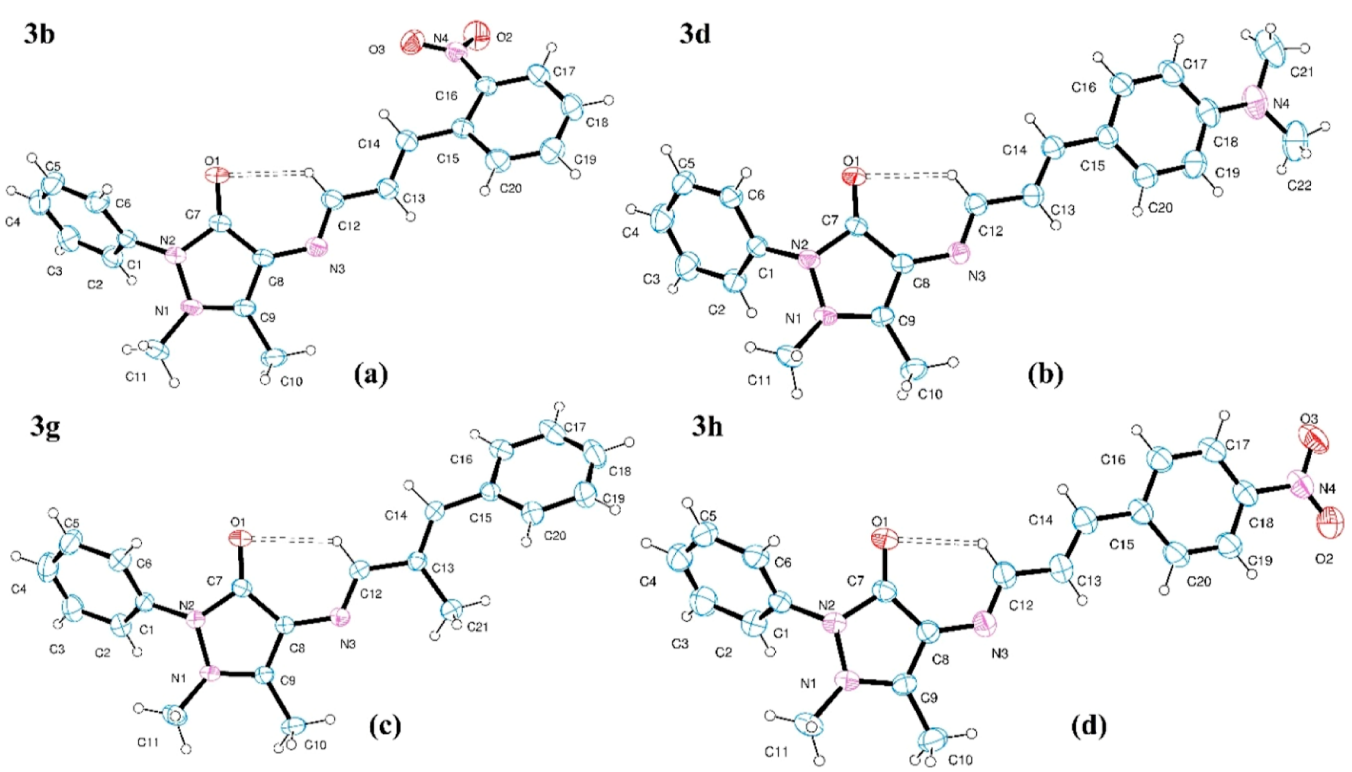

Figure 1. (**a**−**d**) View of **3b**, **3d**, **3g**, and **3h** solid-state molecules showing the labeling of the non-H atoms and their displacement ellipsoids at the 30% probability level. Weak intramolecular CH···O bond is indicated by dashed lines.

and DNA, causing changes in their structure and function;[25,26] as a result, they have great potential as candidates for developing new drugs to treat a wide range of diseases.

The great majority of reports on Schiff bases derived from 4-AAP have concentrated primarily on the use of substituted benzaldehydes, with relatively few reports involving the use of cinnamaldehydes. The presence of a double-bound conjugated with the imino moiety is attractive not only for the synthesis of novel compounds with potential biological activity but also for potential uses in optical applications.[27,28] We recently synthesized several Schiff base derivatives obtained from 4-AAP with various cinnamaldehydes and preliminary data show that these compounds present antibacterial activity and antiproliferative activity against several carcinoma cell lines.[29]

https://doi.org/10.1021/acsomega.3c05372
ACS Omega 2023, 8, 42632−42646

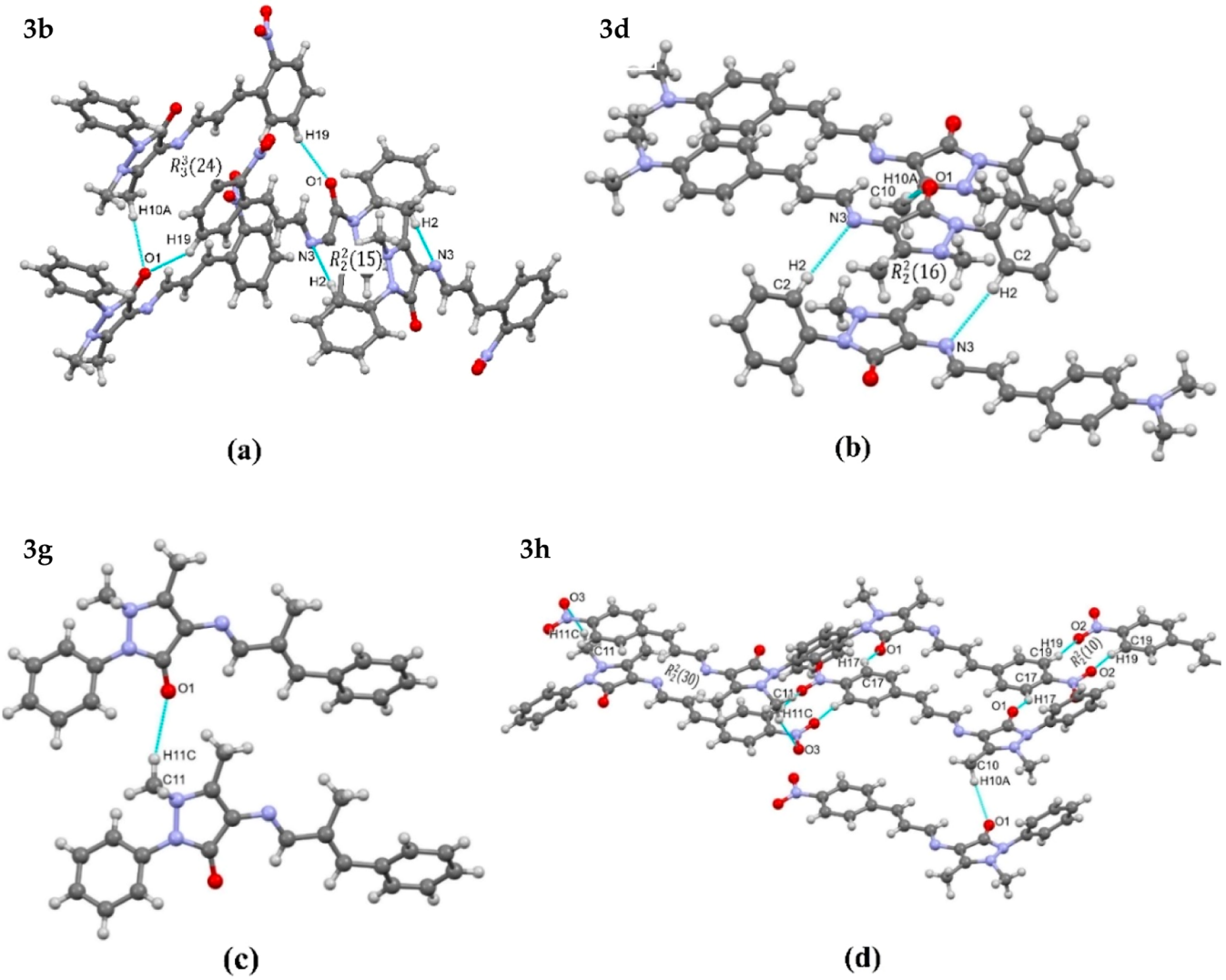

Figure 2. (**a**–**d**) Packing of **3b**, **3d**, **3g**, and **3h** *via* C_{sp3}–H···O, C_{sp2}–H···O, C_{sp3}–H···N, and C_{sp2}–H···N intermolecular interactions.

In order to continue our investigation of these compounds, we report here vibrational (IR), electronic (UV–vis) spectroscopy, electrochemical characterization of these Schiff base derivatives, and X-ray diffraction studies of four compounds. Likewise, the vibrational and electronic spectra were discussed and assigned using theoretical calculations at the PM6/ZDO level of theory. Furthermore, the Hirshfeld surface (HS) analysis was used to investigate their crystal packing and intermolecular interactions to extend and discuss the changes in crystal packing and supramolecular stability observed in related compounds.[30] Lastly, the anti-inflammatory activity, antifungal activity, and biofilm inhibition results are reported.

RESULTS AND DISCUSSION

Schiff bases **3a**–**h** (Scheme 1) were synthesized in good to excellent yield by the condensation of 4-amino-1,5-dimethyl-2-phenylpyrazol-3-one (**1**) with various cinnamaldehydes **2a**–**h** in ethanol, as previously reported.[29] In all cases, the synthesized compounds correspond to *trans* isomers around the side chain olefinic double bond ($J_{\alpha-\beta} \approx 16$ Hz), with no evidence of *cis* isomer formation (see the Experimental Section and Supporting Information, Figures S1–S8).

Crystallographic Structural Results. *Molecular Structures.* Recrystallization in ethanol produced single crystals of four compounds (**3b, 3d, 3g**, and **3h**) that were suitable for crystallographic analysis. Figure 1 is an ORTEP[31] drawing of the solid-state molecules, and their corresponding bond distances and angles are in Tables S1–S6. Although the compounds studied are derivatives of the same molecular framework, their solid-state structures are similar, with the main difference being the angular conformation of the terminal phenyl rings around the corresponding linking C–N and C–C σ-bonds.

Because of extended π-bonding delocalization, the C_{pyr}–N═(CH)–(CR)═(CH)–C_{bz} chain (where R═H for **3b**, **3d**, and **3h**, and R═CH_3 for **3g**), which includes the > C═N– azomethine group of the Schiff base is the planar [*rms* deviation of atoms from the best least-squares plane of 0.055 Å (**3b**), 0.044 Å (**3d**), 0.034 Å (**3g**), and 0.013 Å (**3h**)] and favored by a weak intramolecular CH···O bond, nearly coplanar with the mean plane of the pyrazole ring [angled at 6.3(2)° (**3b**), 7.4(2)° (**3d**), 3.2(1)° (**3g**), and 6.9(2)° (**3h**)]. The phenyl ring attached to the pyrazole ring subtends angles of 61.03(6)° (**3b**), 49.33(6)° (**3d**), 46.75(6)° (**3g**), and 55.39(8)° (**3h**) with it and the phenyl ring at the other molecular end forms angles of 30.0(1)° (**3b**),

https://doi.org/10.1021/acsomega.3c05372
ACS Omega 2023, 8, 42632–42646

Table 1. Potential Hydrogen Bond (Distances in Å; Angles in °) Interactions and Lattice Energies (kJ/mol) for 3b, 3d, 3g, and 3h[a]

D-H···A	d(D-H)	d(H···A)	d(D···A)	∠(D-H···A)	R[c]	E_{ele}	E_{pol}	E_{dis}	E_{rep}	E_{TOT}
compound 3b[b]										
C2−H2···N[i]	0.930	2.600	3.5188(2)	172	6.63	−6.0	−3.6	−42.1	20.8	−29.5
C10−H10A···O1[ii]	0.960	2.490	3.4158(2)	162	6.91	−16.4	−7.6	−29.4	17.3	−34.2
C19−H19···O1[iii]	0.930	2.350	3.1411(2)	142	7.53	−29.3	−14.3	−30.3	18.6	−51.4
C12−H12···O1 (intra)	0.930	2.370	3.0376(2)	129						
C14−H14···O3 (intra)	0.930	2.280	2.8479(2)	119						
compound 3d[b]										
C10−H10A···O1[i]	0.960	2.410	3.3562(3)	167	7.05	−20.8	−7.9	−30.2	16.0	−40.6
C2−H2···N3[ii]	0,930	2.630	3,5180	160	6.98	−32.7	−10.6	−74.0	38.4	−75.7
C12−H12···O1 (intra)	0.930	2.380	3.0463(2)	128						
compound 3g[b]										
C11−H11C···O1[i]	0.960	2.604	3.5300(2)	162	6.91	−16.4	−7.6	−29.4	17.3	−34.2
C10−H10B···N3 (intra)	0.960	2.610	2.9831(3)	103						
C12−H12···O1 (intra)	0.930	2.440	3.0998(3)	128						
compound 3h[b]										
C10−H10A···O1[i]	0.960	2.380	3.3293(3)	172	6.91	−16.4	−7.6	−29.4	17.3	−34.2
C11−H11C···O3[ii]	0.960	2.580	3.4985(3)	160	4.92	−14.6	−6.2	−97.6	44.2	−70.9
C17−H17···O1[iii]	0.930	2.410	3.2295(3)	147	7.53	−29.3	−14.3	−30.3	18.6	−51.4
C19−H19···O2[iv]	0.930	2.460	3.2900(3)	149	15.66	−21.4	−4.9	−10.7	10.7	−25.9
C14−H14···O3 (intra)	0.930	2.370	3.0409(2)	129						

[a]Symmetry code (**3b**): (i) 2 − *x*,− *y*,− *z* (ii) *x*,− 1 + *y*, *z* (iii) 3/2 − *x*,− 1/2 + *y*, 1/2 − *z*. (**3d**): (i) *x*, 1 + *y*, *z* (ii) 1 − *x*,− *y*,− *z*. (**3g**): (i) −1 + *x*, *y*, *z*. (**3h**): (i) *x*, 1 + *y*, *z* (ii) 1 − *x*, 2 − *y*,− *z* (iii) 1 − *x*, 1 − *y*,− *z* (iv) 2 − *x*, 2 − *y*,− *z*. [b]Numbering according to Figure 1. [c]Distance between molecular centroids (mean atomic position) in Å.

6.6(2)° (**3d**), 40.2(1)° (**3g**), and 3.0(2)° (**3h**) with the corresponding chain plane.

Observed bond distances and angles for all four compounds agree with the established organic chemistry rules. For convenience, we shall refer to the metric of the representative and better-refined **3g** compound. In particular, the observed short C−N distance of 1.277(2) Å in the > C═N− azomethine group confirms this link's formal double bond character. Phenyl rings C−C bond distances [from 1.357(3) to 1.394(2) Å] are as expected for a resonant-bond structure. Within the pyrazole ring, observed d(N−N) = 1.412(2) Å, N−C bond distances in the 1.357(2)−1.460(2) Å range and the sum of bond angles around the N-atoms less than 360° [346.6(2) and 352.4(3)°] confirm the single-bond character of the links involving both amine N-atoms. The observed OC-C and short H_3CC═C bond lengths of 1.434(2) and 1.359(2) Å, respectively, are as expected for the single and double bond characters of these links.

The geometrical parameters, such as bond lengths and angles, were also determined theoretically from the most stable conformers of **3b**, **3d**, **3g**, and **3h** at the PM6/ZDO level of theory and were compared using the root-mean-square deviation (rmsd). Tables S23 and S24 show the experimental and calculated bond lengths (Å) and bond angles (deg), while Table S25 shows the calculated standard error values of the bond lengths and angles. The comparative analysis revealed that the theoretical bond lengths **3b**, **3d**, **3g**, and **3h** are in good agreement with the values observed by X-ray diffraction. However, the rmsd for angles evidenced divergence between the theoretical and experimental values due to the theoretical structures determined in the gas phase without evaluating crystal packing effects or intermolecular interactions that can stabilize higher energy conformations and the level of calculation used.

Supramolecular Features and HS Analysis. The crystal packing diagrams for **3b**, **3d**, **3g**, and **3h** are shown in Figure 2a−d. The crystal packing of the compounds is stabilized by intermolecular C_{sp3}−H···O, C_{sp2}−H···O, C_{sp3}−H···N, and C_{sp2}−H···N hydrogen bonds (Table 1). For **3b**, the carbonyl group of the 1*H*-pyrazole moiety arises as bifurcated C10−H10A···O1 (d(H···O) = 2.490 Å, ∠(C−H···O) = 162°) and C19−H19···O1 (d(H···O) = 2.350 Å, ∠(C−H···O) = 142°) hydrogen bonds (Figure 2b). In this sense, the intermolecular contacts between the oxygen atom of the 1*H*-pyrazole with hydrogen atoms of methyl groups and aromatic protons generate the $R_3^3(24)$ graph set. On the other hand, in **3b** and **3d** compounds, the C2−H2···N (d(H···N) = 2.600 Å, ∠(C−H···N) = 172°) and C2−H2···N3 (d(H···N) = 2.630 Å, ∠(C−H···N) = 160°) hydrogen bonds generate structural dimers between nitrogen atoms of the imine group and a hydrogen atom of the benzene moiety that create $R_2^2(15)$ and $R_2^2(16)$ motifs, respectively (Figure 2a,b).

For **3h**, the crystal packing is stabilized by $R_2^2(10)$ and $R_2^2(30)$ graph-set ring motifs, which form dimers in the supramolecular assembly (Figure 2d). These intermolecular interactions C19−H19···O2 (d(H···O) = 2.460 Å, ∠(C−H···O) = 149°) and C11−H11C···O3 (d(H···O) = 2.580 Å, ∠(C−H···O) = 160°) evidences the important participation of hydrogen atoms of methyl groups and a benzyl moiety with oxygen atoms of the $-NO_2$ group. Likewise, for **3d**, **3g**, and **3h**, the 1*H*-pyrazole moiety generates C−H···O intermolecular interactions that stabilized the crystalline packing by hydrogen bonds C10−H10A···O1, C11−H11C···O1, and C17−H17···O1 between hydrogen atoms of the $-CH_3$ group and oxygen of the carbonyl group.

On the other hand, intermolecular interactions of type $\pi\cdots\pi$ stacking, C−H···π, and C═O···π were evidenced for **3b**, **3d**, **3g**, and **3h** (Figures S17−S20, Supporting Information). The C−H···π intermolecular interactions for **3b**, **3g**, and **3h** evidenced a close distance of contact (Comp. **3b**: 2.921 and 2.901 Å, Comp. **3g**: 2.897 Å and 2.911 Å, and Comp. **3h**: 2.988 Å) where the interaction arises principally between hydrogen atoms of the

https://doi.org/10.1021/acsomega.3c05372
ACS Omega 2023, 8, 42632−42646

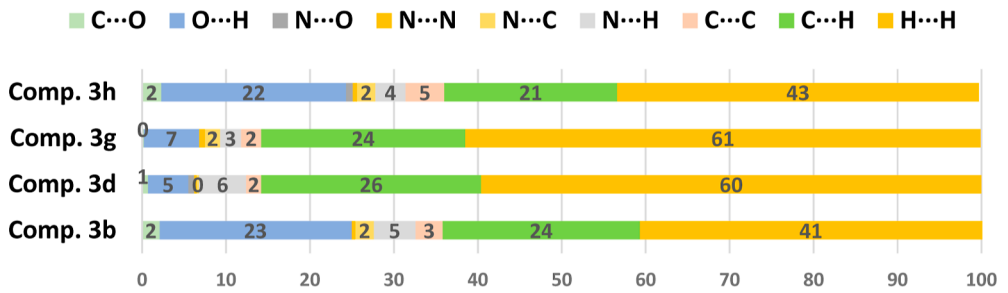

Figure 3. Relative (%) contributions of the main intermolecular contacts to the HS areas for compounds **3b**, **3d**, **3g**, and **3h**.

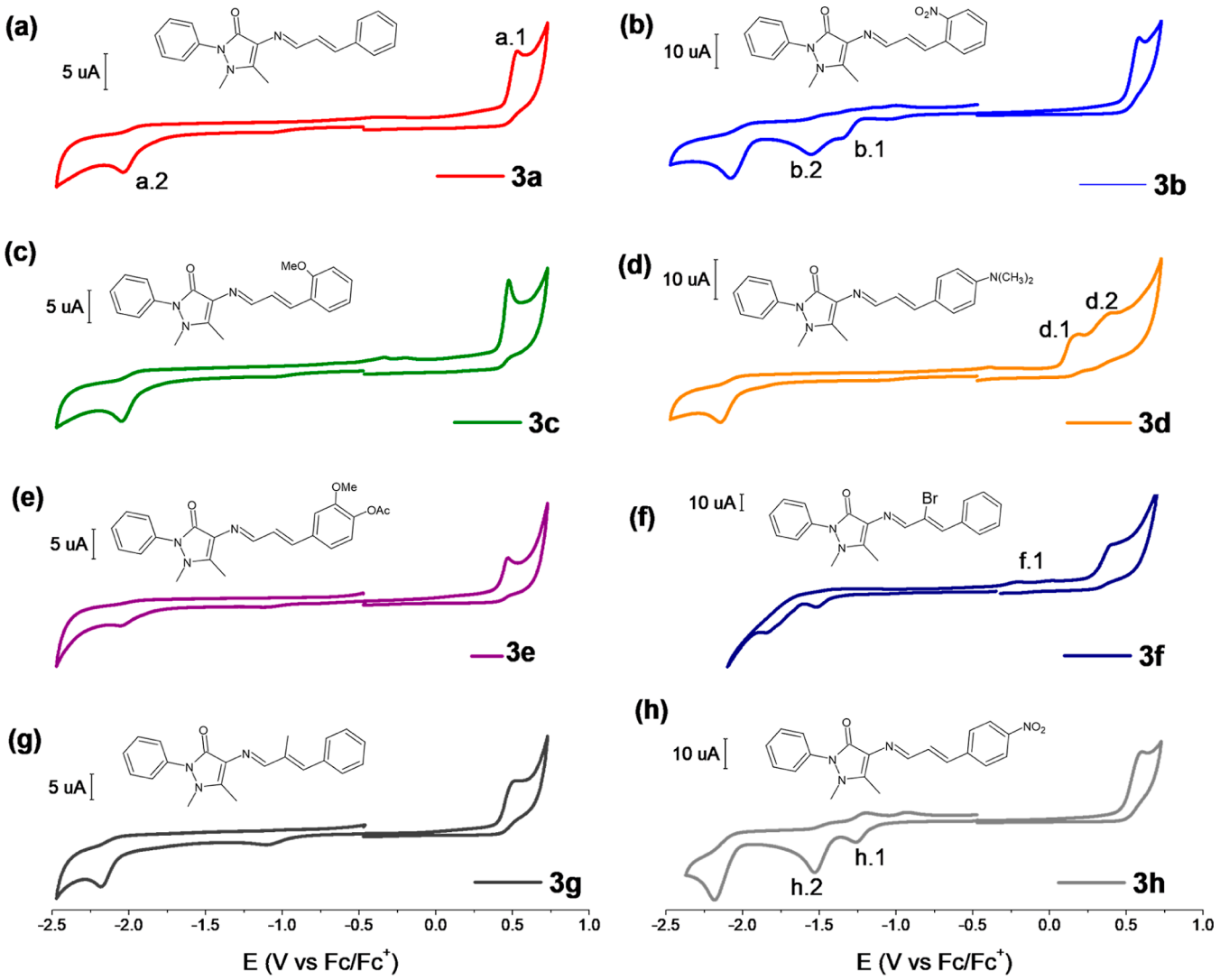

Figure 4. Voltammograms of Schiff-base derivatives **3a**−**h** in DMSO (1.0 mM) + 0.1 M tetramethylammonium perchlorate at a scan rate of 100 mV/s.

benzene moiety. For **3b**, **3d**, and **3g**, the intermolecular π stacking contacts (Figures S17−S19, Supporting Information) are observed between the 1*H*-pyrazole rings (intercentroid distances: Comp. **3b**: 4.162 Å, Comp. **3d**: 4.127 Å, and Comp. **3g**: 3.890 Å). Moreover, interactions $\pi\cdots\pi$ stacking arise between the 1*H*-pyrazole moiety and the benzene ring for **3b** and **3h** (intercentroid distances: Comp. **3b**: 3.996 Å and Comp. **3h**: 3.646 Å). Likewise, for **3d** and **3g**, we observed C═O$\cdots\pi$ intermolecular interactions between 1*H*-pyrazole rings (intercentroid distances: Comp. **3b**: 3.123 Å and Comp. **3g**: 3.905 Å).

The features associated with the energy of each intermolecular interaction shown in Tables S26−S29 were evaluated by the Crystal Explorer program, applying the CE-HF/3-21G energy model for the electron densities. Figures S21−S24 show the detailed crystal lattice analysis and 3D-energy frameworks. The analysis of **3b**, **3d**, **3g**, and **3h** evidenced that the C−H···O hydrogen bonds are dominated mainly by dispersive energies with values in a range of −97.6−−29.4 kJ mol^{-1} and electrostatic energy contributions in a range of −32.7−−14.6 kJ mol^{-1}. Moreover, compounds **3b** and **3d** show C−H···N hydrogen bonds, where the nature of the interactions evidenced

https://doi.org/10.1021/acsomega.3c05372
ACS Omega 2023, 8, 42632−42646

Table 2. Experimental and Calculated Frequencies (cm^{-1}) and Tentative Assignment of the Most Relevant Vibrational Modes for 3a−3h

compound 3a				compound 3b			
assignment PED (%)[a]	Exp.	Calc.[c]		assignment PED (%)[a]	Exp.	Calc.[c]	
	IR[b]	Freq.	Int.		IR[b]	Freq.	Int.
ν_s (C−H) (86) $_{Ar}$	3045 (vw)	2768	250	ν_s (C−H) (88) $_{Ar}$	3052 (vw)	2758	324
ν_{as} (C−H) (91) $_{Ar}$	3035 (vw)	2759	267	ν_{as} (C−H) (96) $_{Ar}$	3019 (vw)	2719	145
ν_{as} (CH_3) (84) $_{pyrazole}$	3001 (vw)	2678	175	ν_{as} (CH_3) (97) $_{pyrazole}$	2961 (vw)	2677	122
ν_{as} (CH_3) (88) $_{pyrazole}$	2960 (vw)	2659	118	ν_{as} (CH_3) (88) $_{pyrazole}$	2846 (vw)	2658	80
ν (C−H) (91) $_{azomethine}$	2928 (vw)	2626	105	ν (C═O) (87) $_{pyrazole}$	1643 (vs)	1859	422
ν (C═O) (89) $_{pyrazole}$	1643 (vs)	1859	891	ν (C═C) (83) $_{alkene}$	1607 (w)	1776	24
ν (C═C) (81) $_{alkene}$	1594 (m)	1776	9	ν (C═N) (84) $_{azomethine}$	1592 (w)	1721	21
ν (C═N) (77) $_{azomethine}$	1587 (m)	1722	5	ν_{as} (NO_2) (91)	1569 (s)	1706	839
ν (C═C) (69) $_{pyrazole}$	1558 (m)	1657	368	ν (C═C) (63) $_{pyrazole}$	1557 (m)	1649	319
δ (C−C−H) (31) ip $_{Ar}$	1415 (m)	1509	282	δ (C−C−H) (32) ip $_{Ar}$	1510 (m)	1509	293
ν (C−N) (53) $_{pyrazole}$	1455 (w)	1413	307	ν_s (NO_2) (74)	1444 (w)	1441	420
ν (N−N) (61) $_{pyrazole}$	1447 (w)	1388	345	ν (C−N) (52) $_{pyrazole}$	1428 (w)	1417	435
δ (CH_3) (35) $_{pyrazole}$	1307 (m)	1298	26	ν (N−N) (52) $_{pyrazole}$	1413 (w)	1390	340
δ (C−C−N) (35) $_{pyrazole}$	1133 (m)	1169	438	δ (CH_3) (29) $_{pyrazole}$	1077 (w)	1077	77
δ (N−C−H) (56) $_{pyrazole}$	1045 (w)	1056	72	δ (C−C−H) (63) $_{pyrazole}$	978 (m)	970	5
δ (CH_3) (60) $_{pyrazole}$	1117 (s)	1017	60				
δ (C−C−H) (78) $_{pyrazole}$	858 (vw)	963	85				

compound 3c				compound 3d			
assignment PED (%)[a]	Exp.	Calc.[c]		assignment PED (%)[a]	Exp.	Calc.[c]	
	IR[b]	Freq.	Int.		IR[b]	Freq.	Int.
ν_s (C−H) (94) $_{Ar}$	3035 (vw)	2769	245	ν_s (CH_3) (34) $_{pyrazole}$	3039 (vw)	2779	77
ν_{as} (C−H) (89) $_{Ar}$	3007 (vw)	2763	259	ν_s (CH_3) (19) $_{pyrazole}$	2961 (vw)	2762	74
ν_s (C−H) (76) $_{Alkene}$	2960 (vw)	2745	214	ν_{as} (C−H) (63) $_{Ar}$	2926 (vw)	2758	235
ν_{as} (CH_3) (93) $_{pyrazole}$	2681 (vw)	2737	28	ν_{as} (C−H) (53) $_{Ar}$	2892 (vw)	2752	233
ν_{as} (CH_3) (89) $_{pyrazole}$	2812 (vw)	2735	92	ν_{as} (C−H) (90) $_{Ar}$	2853 (vw)	2735	93
ν (C═O) (86) $_{pyrazole}$	1643 (vs)	1851	904	ν_s (CH_3) (29) $_{N,N\text{-}dimethyl}$	2810 (vw)	2673	94
ν (C═C) (78) $_{alkene}$	1614 (w)	1772	102	ν_{as} (CH_3) (28) $_{N,N\text{-}dimethyl}$	2797 (vw)	2664	74
ν (C═N) (79) $_{azomethine}$	1594 (w)	1737	274	ν (C═O) (86) $_{pyrazole}$	1643 (s)	1850	418
ν (C═C) (74) $_{pyrazole}$	1579 (w)	1686	606	ν (C═N) (47) $_{azomethine}$	1600 (s)	1737	139
ν (C−N) (36) $_{pyrazole}$	1435 (w)	1406	96	ν (C═C) (34) $_{pyrazole}$	1564 (m)	1647	533
δ (CH_3) (74) $_{methoxy}$	1414 (w)	1385	631	ν (C−N) (30) $_{N,N\text{-}dimethyl}$	1434 (m)	1440	250
ν (N−N) (19) $_{pyrazole}$	1413 (w)	1361	320	ν (C−N) (22) $_{pyrazole}$	1407 (w)	1404	146
δ (CH_3) (80) $_{pyrazole}$	1381 (w)	1331	72	ν (N−N) (27) $_{pyrazole}$	1368 (s)	1385	375
δ (C═C−H) (74) $_{azomethine}$	1346 (vw)	1294	139	δ_s (CH_3) (19) $_{N,N\text{-}dimethyl}$	1314 (w)	1353	37
δ (C−C−H) (48) ip $_{Ar}$	1510 (m)	1245	76	δ (CH_3) (34) $_{pyrazole}$	1288 (m)	1332	79
δ (O−C−H) (51) $_{methoxy}$	1074 (vw)	1069	1	δ (C═C−H) (22) $_{azomethine}$	1239 (vw)	1294	58
δ (CH_3) (52) $_{pyrazole}$	1050 (w)	1062	46	δ_{as} (CH_3) (27) $_{N,N\text{-}dimethyl}$	1184 (w)	1252	61
δ (C−C−H)(46) oop $_{alkene}$	991 (m)	967	43	δ_{as} (CH_3) (18) $_{N,N\text{-}dimethyl}$	1023 (m)	1024	74
				δ (C−C−H) (20) oop $_{alkene}$	946 (m)	951	72

compound 3e				compound 3f			
assignment PED (%)[a]	Exp.	Calc.[c]		assignment PED (%)[a]	Exp.	Calc.[c]	
	IR[b]	Freq.	Int.		IR[b]	Freq.	Int.
ν_s (C−H) (26) $_{Ar}$	3028 (vw)	2769	117	ν_{as} (CH_3) (36) $_{ketone}$	3103 (vw)	2778	83
ν_{as} (C−H) (57) $_{Ar}$	3011 (vw)	2758	186	ν_s (C−H) (41) $_{Ar}$	3067 (vw)	2768	229
ν_{as} (C−H) (62) $_{Ar}$	2979 (vw)	2752	123	ν_{as} (C−H) (49) $_{Ar}$	3054 (vw)	2759	242
ν_{as} (CH_3) (52) $_{acetoxy}$	2941 (vw)	2684	123	ν_{as} (C−H) (89) $_{Ar}$	3042 (vw)	2735	93
ν_{as} (CH_3) (51) $_{pyrazole}$	2916 (vw)	2678	116	ν (C−H) (98) $_{ketone}$	3029 (vw)	2728	134
ν_{as} (CH_3) (77) $_{acetoxy}$	2876 (vw)	2651	119	ν_{as} (CH_3) (65) $_{ketone}$	2995 (vw)	2678	106
ν_s (C−H) (48) $_{azomethine}$	2828 (vw)	2624	74	ν_{as} (CH_3) (56) $_{pyrazole}$	2942 (vw)	2659	86
ν (C═O) (88) $_{ester}$	1755 (vs)	1860	421	ν (C═O) (88) $_{pyrazole}$	1645 (vs)	1857	393
ν (C═O) (88) $_{pyrazole}$	1744^{sh} (m)	1843	710	ν (C═N) (69) $_{azomethine}$	1608 (w)	1728	13
ν (C═N) (77) $_{azomethine}$	1655 (w)	1722	12	ν (C═C) (66) $_{pyrazole}$	1591 (m)	1666	294
ν (C═C) (56) $_{pyrazole}$	1640 (m)	1652	383	δ (C−C−H) (35) ip $_{Ar}$	1567 (w)	1641	100
δ (C−C−H) (16) ip $_{Ar}$	1594 (m)	1509	308	ν (C−N) (17) $_{pyrazole}$	1492 (m)	1509	276
ν (C−N) (17) $_{pyrazole}$	1509 (m)	1418	257	ν (C−N) (22) $_{pyrazole}$	1509 (w)	1412	246
ν (N−N) (26) $_{pyrazole}$	1483 (m)	1389	271	ν (N−N) (25) $_{pyrazole}$	1417 (m)	1388	316

https://doi.org/10.1021/acsomega.3c05372
ACS Omega 2023, 8, 42632−42646

Table 2. continued

compound 3e				compound 3f			
assignment PED (%)[a]	Exp.	Calc.[c]		assignment PED (%)[a]	Exp.	Calc.[c]	
	IR[b]	Freq.	Int.		IR[b]	Freq.	Int.
δ (CH_3) (17) $_{pyrazole}$	1467 (m)	1368	131	δ (CH_3) (38) $_{pyrazole}$	1337 (m)	1332	76
δ (CH_3) (38) $_{pyrazole}$	1368 (m)	1330	75	δ (C=C−H) (48) $_{azomethine}$	1225 (vw)	1266	21
δ (CH_3) (38) $_{acetoxy}$	1344 (m)	1312	123	δ (CH_3) (45) $_{pyrazole}$	1178 (w)	1242	31
δ (CH_3) (17) $_{acetoxy}$	1289 (m)	1212	354	δ (CH_3) (39) $_{pyrazole}$	1137 (m)	1129	52
δ (CH_3) (28) $_{methoxy}$	1212 (m)	1123	68	δ (C=C−H) (18) $_{alkene}$	1075 (w)	1194	41
δ (CH_3) (36) $_{methoxy}$	1125 (s)	1030	64	δ (CH_3) (29) $_{pyrazole}$	942 (m)	1057	52
δ (C−C−H)(28) oop $_{alkene}$	1032 (s)	959	82	δ (CH_3) (29) $_{pyrazole}$	926 (w)	1018	57
ν (C−O) (37) $_{ester}$	993 (vs)	940	115	ν (C−Br) (20)	627 (w)	614	60
compound 3g				**compound 3h**			
assignment PED (%)[a]	Exp.	Calc.[c]		assignment PED (%)[a]	Exp.	Calc.[c]	
	IR[b]	Freq.	Int.		IR[b]	Freq.	Int.
ν_s (CH_3) (34) $_{pyrazole}$	3145 (vw)	2779	82	ν_s (C−H) (27) $_{Ar}$	3117 (vw)	2768	117
ν_s (C−H) (50) $_{Ar}$	3099 (vw)	2768	156	ν_{as} (C−H) (56) $_{Ar}$	3100 (vw)	2756	192
ν_{as} (C−H) (37) $_{Ar}$	3067 (vw)	2761	239	ν_{as} (C−H) (55) $_{Ar}$	3071 (vw)	2749	210
ν_{as} (C−H) (39) $_{Ar}$	3052 (vw)	2753	111	ν_{as} (C−H) (80) $_{Ar}$	3031 (vw)	2724	137
ν_{as} (C−H) (31) $_{ketone}$	3040 (vw)	2748	76	ν_{as} (C−H) (76) $_{Ar}$	3022 (vw)	2722	113
ν_{as} (C−H) (89) $_{Ar}$	3026 (vw)	2735	92	ν_{as} (CH_3) (42) $_{pyrazole}$	2997 (vw)	2677	84
ν_{as} (CH_3) (58) $_{alkene}$	2984 (vw)	2691	84	ν_{as} (CH_3) (47) $_{pyrazole}$	2975 (vw)	2657	84
ν_{as} (CH_3) (65) $_{pyrazole}$	2959 (vw)	2679	77	ν (C−H) (49) $_{alkene}$	2928 (vw)	2624	76
ν_{as} (CH_3) (55) $_{alkene}$	2943 (vw)	2675	97	ν (C=O) (81) $_{pyrazole}$	1646 (vs)	1861	417
ν_{as} (CH_3) $_{pyrazole}$	2919 (vw)	2661	79	ν (C=N) (78) $_{azomethine}$	1612^{sh} (w)	1718	54
ν (C=O) (86) $_{pyrazole}$	1641 (vs)	1850	427	ν (NO_2) (48)	1594 (s)	1714	586
ν (C=N) (74) $_{azomethine}$	1618^{sh} (w)	1758	19	ν (C=C) (41) $_{pyrazole}$	1568 (s)	1645	158
ν (C=C) (58) $_{pyrazole}$	1588 (s)	1688	194	δ (C−C−H) (25) ip $_{Ar}$	1549 (m)	1634	626
δ (C−C−H) (35) ip $_{Ar}$	1571 (w)	1641	88	ν (C−N) (16) $_{pyrazole}$	1511 (s)	1508	278
δ (C−C−H) (16) ip $_{Ar}$	1494 (m)	1527	40	ν (NO_2) (42)	1433 (m)	1443	725
δ (C−C−H) (17) ip $_{Ar}$	1481 (m)	1510	272	ν (N−N) (23) $_{pyrazole}$	1420 (w)	1392	286
ν (C−N) (24) $_{pyrazole}$	1418 (m)	1409	103	ν (C−N) (14) $_{azomethine}$	1410 (w)	1378	170
ν (N−N) (27) $_{pyrazole}$	1387 (w)	1387	290	δ (CH_3) (19) $_{pyrazole}$	1377 (w)	1353	66
δ (C=C−H) (23) $_{alkene}$	1371 (w)	1370	99	δ (CH_3) (17) $_{pyrazole}$	1335 (w)	1334	92
δ (CH_3) (23) $_{alkene}$	1313^{sh} (w)	1342	90	δ (CH_3) (37) $_{pyrazole}$	1250 (w)	1217	75
δ (CH_3) (18) $_{alkene}$	1302 (m)	1336	85	δ (C=C−H) (44) $_{alkene}$	972 (m)	958	92
δ (C=C−H) (76) $_{azomethine}$	1191 (vw)	1282	13	δ (NO_2) (31)	871 (m)	808	92
δ (CH_3) (51) $_{pyrazole}$	1176 (w)	1244	43	δ (NO_2) (37) oop	826 (m)	764	109
δ (CH_3) (39) $_{pyrazole}$	1154 (w)	1229	52	δ (NO_2) (39) ip	534 (w)	527	2

[a] ν, δ, y, and γ represent stretching, in-plane deformation (ip), and out-of-plane deformation (op) vibrational modes, respectively. In parentheses, potential energy distribution (PED) analysis. [b] vs, very strong; s, strong; m, medium; w, weak; vw, very weak; and sh, shoulder. [c] Calculated infrared frequencies (cm^{-1}) and intensities (km mol^{-1}) in parentheses (B3LYP/6-311++G(d,p).

dispersive and repulsive contributions of energy (Comp. **3b**: E_{dis}: −42.1 kJ mol^{-1} and E_{rep}: −20.8 kJ mol^{-1}; Comp. **3d**: E_{dis}: −74.0 kJ mol^{-1} and E_{rep}: −38.4 kJ mol^{-1}).

The HS analysis was performed to explore the relative contribution of each intermolecular interaction in the crystal packing. Figures S25−S28 (row A) show small contacts or intermolecular interactions on the d_{norm} surface, as highlighted in red dots. The red circular regions on the d_{norm} surfaces are indicative of C_{sp3}−H···O, C_{sp2}−H···O, C_{sp3}−H···N, and C_{sp2}−H···N hydrogen bonds and other contacts, where the carbonyl group (C=O) and methyl group (−CH_3) of the 1*H*-pyrazole ring; moreover, the benzyl, imine, and nitro moieties promote intermolecular interactions in the studied compounds. Likewise, the shape index [Figures S25−S28 (row B)] evidence π···π stacking by "bow-tie" patterns that are observed as red and blue triangles over the surface, while C−O···π and C=O···π interactions are also evident as large and flat green regions delineated by a blue outline over the curvedness surface [Figures S25−S28 (row C)]. On the other hand, Figure S29 shows 2D-fingerprint plots that allowed rationalization of the contribution of significant intermolecular interactions in the crystalline arrangements. In this sense, the H···H contacts have the most significant contribution to the total HS, with 41, 60, 61, and 43% for **3b**, **3d**, **3g**, and **3h**, respectively (Figure 3). Moreover, the H···H contacts also contribute to the HS with moderate contributions of 24, 26, 24, and 21%. This result reveals that the close planarity of the molecular structures contributes to the relatively high proportion of H···H and C···H contacts, related to π···π stacking and C−H···π and C=O···π weak intermolecular interactions that contribute to stabilizing the crystalline packing. Besides, the C−H··· O intermolecular hydrogen bonds show relative contributions for **3b** and **3h** with 23 and 22%, respectively, due to the −NO_2 groups.

Electrochemical Characterization. Electrochemistry is a powerful tool to probe reactions involving electron transfers.[32] Cyclic voltammetry (CV) is an electroanalytical technique

https://doi.org/10.1021/acsomega.3c05372
ACS Omega 2023, 8, 42632−42646

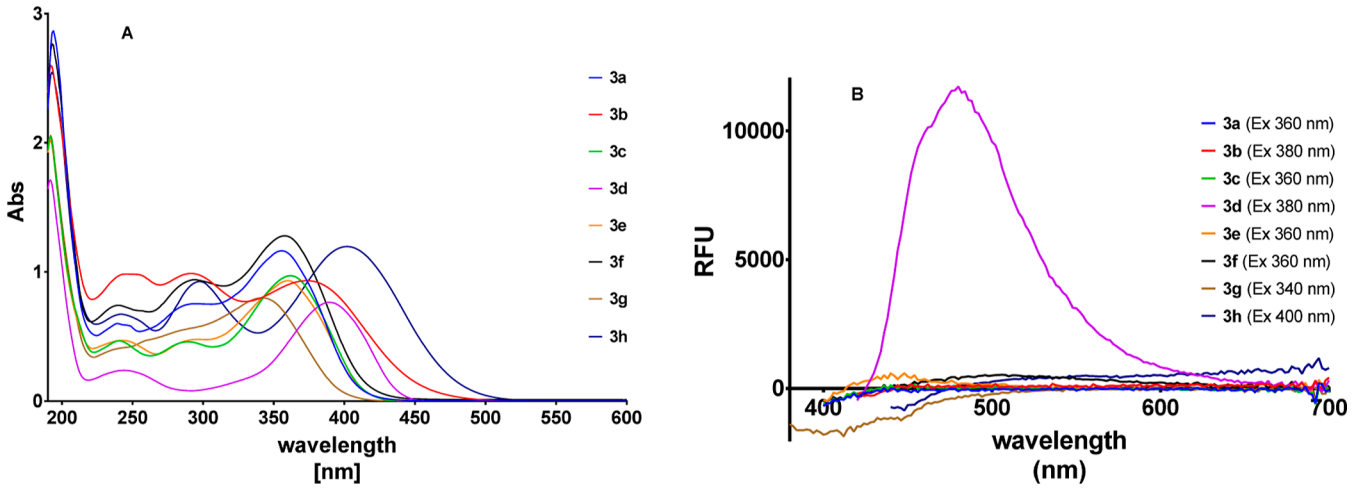

Figure 5. (A) Electronic absorption spectra of Schiff bases **3a**−**3h** using acetonitrile as the solvent (**3a**: 60 μM, **3b**: 35 μM, **3c**: 25 μM, **3d**: 12.5 μM, **3e**: 25 μM, **3f**: 45 μM, **3g**: 30 μM, and **3h**: 70 μM). (B) Emission spectra of Schiff bases **3a**−**3h** in acetonitrile at room temperature.

employing a triangular potential waveform to identify species, equilibria, binding properties, and oxidation estates of organic, inorganic, and organometallic compounds.[33] The electrochemical behaviors of the Schiff bases were studied using the CV technique in a DMSO solution containing 0.1 M NMe_4ClO_4. Figure 4 shows voltammograms of all synthesized Schiff-base derivatives. First, in Figure S30, we showed the potential window and background for all derivatives, from −2.5 to 0.73 V *vs* ferrocene/ferrocenium, with a little signal at −1.079 V *vs* Fc/Fc^+ due to oxygen reduction. The voltammogram of Figure 4a shows data from compound **3a**, the base structure of the derivative family, exhibiting two irreversible peak signals. The peak at $E_{p,a}$ = 0.526 V *vs* Fc/Fc^+, can be attributed to the oxidation that takes place at the amino group of the dipyrone ring,[34] while the reduction one at $E_{p,c}$ = −2.030 V *vs* Fc/Fc^+, can be assigned to imine reduction.[35] The voltammogram of **3b** (Figure 4b) has two extra irreversible reduction signals labeled as b.1 at $E_{p,c}$ = 1.343 V and b.2 at $E_{p,c}$ = −1.571. These signals correspond to the reduction of the nitro group; the first step in aprotic media includes one electron interchange to get the radical anion $R\text{-}NO_2^-$, then the second electron transfer occurs to obtain the dianion species $R\text{-}NO_2^{2-}$.[36] Figure 4c shows data from Schiff base **3d**, which has the same shape as **3a**, with an oxidation peak at 0.474 V and an irreversible reduction signal at −2.030 V. In the voltammogram of **3d** (Figure 4d), one extra irreversible oxidation peak, labeled as d.1, is found at $E_{p,a}$ = 0.147 V, and is attributed to amine group oxidation. Schiff bases **3e** and **3g** show voltammograms similar to **3a** (Figure 4e,g), with one oxidation peak at 0.466 and 0.492 V and a reduction peak at −2.043 and −2.174 V *vs* Fc/Fc^+, respectively. The voltammogram of Schiff base **3f** (Figure 4f) shows an additional peak at −0.115 V *vs* Fc/Fc^+, which can be attributable to the bromine atom, and a diminution of 210 mV in the oxidation signal of the amino group of the dipyrone ring. Finally, the voltammogram of **3g** (Figure 4g) shows two irreversible signals, g.1 at −1.256 V and g.2 at −1.529 V *vs* ferrocene/ferrocenium; these peaks are due to the reduction of the nitro group, which behaves similarly to structure **3b**.

IR Spectroscopy. Figures S9−S16 show the experimental IR spectra of **3a**−**3h** in the solid state. Theoretical calculations for the most stable conformers at the PM6/ZDO level of theory assisted in the tentative assignments of the most relevant vibrational modes. Table 2 shows the unscaled theoretical vibrational frequency of the most representative bands discussed below.

The IR spectra (**3a**−**3h**) show a set of weak absorption bands in the 3145 to 2797 cm^{-1} region, which are attributed to stretching C−H vibrational modes, both symmetric and asymmetric due to the aromatic, methyl, and alkene groups. Strong absorption bands at 1643 cm^{-1} (**3a**−**3d**), 1744 cm^{-1} (**3e**), 1645 cm^{-1} (**3f**), 1641 cm^{-1} (**3g**), and 1646 cm^{-1} (**3h**), are attributed to the carbonyl of the pyrazole ring, as previously reported for related molecules.[37,38] The shift of the C═O band toward lower frequencies in the IR spectra could be explained by the short intermolecular interactions C_{sp2}−O···H−C_{sp3} observed in the supramolecular features in the crystalline structures of **3b**, **3d**, **3g**, and **3h**. The stretching C═C of the pyrazole group appears as medium absorption bands at 1558, 1557, 1579, 1564, 1640, 1591, 1588, and 1568 cm^{-1}, while the weak and medium absorption bands at 1455, 1428, 1435, 1407, 1509, 1492, 1418, and 1410 cm^{-1} were attributed to stretching C−N. Finally, stretching N−N is assigned to weak absorption bands at 1447, 1413, 1413, 1368, 1468, 1483, 1417, 1387, and 1420 cm^{-1}. All these characteristic absorption bands for the pyrazole group are in good agreement with related compounds.[37−40]

The vibration corresponding to the azomethine −CH═N group characterizes the Shiff base. The C═N stretching vibrational mode was attributed to the weak absorption bands at 1587, 1592, 1594, 1600, 1655, 1608, 1618, and 1612 cm^{-1}, for **3a**−**3h**, analogous to the weak absorption bands reported for similar compounds.[39,40]

On the other hand, the IR spectra of **3b**−**3e** and **3h** showed distinctive absorption bands for all different substituents of the benzyl moiety. For **3b** and **3h**, the $-NO_2$ group exhibited significant absorption bands at 1569 cm^{-1} and 1594 m^{-1}, respectively, attributed to a stretching vibrational mode. The methoxy group in **3b** showed a weak absorption band at 1414 cm^{-1}, which was assigned to the bending O−C−H vibrational mode. For **3d**, the C−N stretching was assigned to a weak absorption band at 1407 cm^{-1}, whereas bands at 1314, 1184, and 1023 cm^{-1} were assigned to symmetric and antisymmetric vibrational modes. The absorption bands at 1755, 1334, 1289, and 1125 cm^{-1} in the **3e** IR spectra indicated vibrational modes attributable to stretching of C═O and deformations of the $-CH_3$ moiety of the acetoxy and methoxy groups, respectively. In the case of Schiff bases with an α carbon substitution, **3f** exhibits

https://doi.org/10.1021/acsomega.3c05372
ACS Omega 2023, 8, 42632−42646

Table 3. Experimental and Calculated Electronic Spectra (in nm) of 3a−3h and Tentative Assignment of the Absorption Bands

compound 3a			compound 3b		
Exp.[a]	Calc.[b]	assignment[c]	Exp.	Calc.	assignment
195	253 (0.239)	H-3 → L+1 (26%)	194	263 (0.222)	H-2 → L+5 (11%)
	257 (0.203)	H-4 → L+2 (35%)		272 (0.019)	H-3 → L+7 (9%)
	262 (0.176)	H → L+8 (22%)		273 (0.191)	H → L+9 (13%)
240	318 (0.419)	H-1 → L+1 (15%)	243	318 (0.379)	H-1 → L+2 (12%)
286	390 (0.060)	H → L+5 (43%)	299	391 (0.076)	H → L+8 (43%)
357	464 (0.518)	H → L(50%)	381	466 (0.519)	H → L+1 (27%)
compound 3c			compound 3d		
Exp.	Calc.	assignment	Exp.	Calc.	assignment
193	257 (0.204)	H-4 → L+3 (31%)	193	257 (0.204)	H-4 → L+3 (31%)
	263 (0.170)	H → L+10 (20%)		263 (0.157)	H-2 → L+10 (14%)
	276 (0.238)	H-1 → L+2 (16%)		279 (0.149)	H-5 → L+3 (27%)
242	327 (0.412)	H-3 → L (14%)	245	331 (0.299)	H-2 → L+1 (17%)
291	371 (0.095)	H → L+1 (19%)	392	488 (0.568)	H → L (36%)
365	465 (0.432)	H → L (30%)			
compound 3e			compound 3f		
Exp.	Calc.	assignment	Exp.	Calc.	assignment
192	268 (0.179)	H-4 → L+2 (13%)	194	284 (0.068)	H-5 → L (10%)
	289 (0.204)	H-7 → L+2 (7%)		290 (0.090)	H → L+3 (13%)
243	394 (0.040)	H-2 → L+2 (21%)	241	325 (0.343)	H-1 → L+1 (23%)
291	436 (0.072)	H → L (16%)	294	382 (0.108)	H → L+7 (23%)
363	477 (0.508)	H → L (34%)	360	462 (0.335)	H → L (36%)
compound 3g			compound 3h		
Exp.	Calc.	assignment	Exp.	Calc.	assignment
193	315 (0.518)	H-1 → L+1 (20%)	194	276 (0.076)	H-8 → L+7 (67%)
344	430 (0.250)	H → L (29%)		286 (0.099)	H → L+11 (18%)
				295 (0.109)	H-1 → L+6 (25%)
			243	322 (0.438)	H-9 → L (30%)
			297	394 (0.053)	H → L+6 (51%)
			402	474 (0.620)	H → L (22%)

[a]Absorption maxima and spectral positions are given in nm. [b]Oscillator strengths of calculated transitions, shown in parentheses, are in atomic units. [c]H: HOMO and L: LUMO.

a weak absorption band at 627 cm^{-1} assigned to the stretching C−Br deformation mode, whereas **3g** exhibits a medium absorption band at 1312 cm^{-1} attributable to the $-CH_3$ deformation mode.

Optical Properties. The experimental electronic absorption spectra of **3a−3h** are shown in Figure 5A, while the analyses of the calculated and experimental electronic absorption spectra of all Schiff bases are shown in Table 3. Electronic spectra were calculated at the TD-PM6/ZDO level of theory, while the molecular orbitals involved in the electronic transitions **3a − 3h** are shown in Figures S31−S38.

The experimental electronic spectra **3a−3h** showed strong absorption bands from 192 to 195 nm. The electronic transitions in this range involve principally the participation of $\pi \rightarrow \pi^*$ orbitals for **3a**, **3b**, **3f**, and **3h** due to H-3 → L+1, H-2 → L+5, H → L+3, and H-1 → L+6 excitations, respectively. These strong absorption bands arise by electronic transitions from the π-bonding orbitals of the benzene, 1*H*-pyrazole, azomethine, and double bond of the alkene moiety to π^*-antibonding orbitals of the benzene ring. On the other hand, for the compounds **3c**, **3d**, **3e**, and **3g** that are present in the chemical structure $-O-CH_3$, $-N(CH_3)_3$, $-OCH_3/-OCOCH_3$, and CH_3 groups, the absorption electronic transitions arise by $\pi \rightarrow \pi^*$ orbitals and $n \rightarrow \pi^*$ orbitals, where the strong absorption bands show the participation of nonbonding contributions of the nitrogen of the 1*H*-pyrazole and azomethine groups.

The electronic spectra (**3a−3f** and **3h**) showed weak absorption bands in the 240−245 nm region. The electronic transitions of **3a−3f** involve the participation of $\pi \rightarrow \pi^*$ orbitals, where the π-bonding orbitals along the system of Schiff base derivatives of 4-AAP show participation and transit to π^*-antibonding orbitals of the benzene and 1*H*-pyrazole rings. The weak absorption band at 243 nm in the spectrum of **3h** can be attributed to $n \rightarrow \pi^*$, where the transition arises from nonbonding contributions localized in the oxygen atoms of the $-NO_2$ group.

On the other hand, for **3a−3c**, **3e−3f**, and **3h**, the electronic spectra showed weak bands in a range of 286−299 nm. The electronic transitions arise from $\pi \rightarrow \pi^*$ orbitals, where the π-bonding orbitals of the aromatic system benzene, 1*H*-pyrazole, and azomethine moiety transit to π^*-antibonding orbitals localized principally in the benzene and 1*H*-pyrazole rings. Moreover, the electronic spectra showed a weak broadband range of 342−402 nm for all compounds **3a−3h**. These absorption bands arise mainly from HOMO → LUMO transitions, where the π-bonding orbitals of the aromatic system transit to π^*-antibonding orbitals localized in the 1*H*-pyrazole, azomethine, and double bonds of the alkene moiety. Interestingly, none of the Schiff bases present emission when

https://doi.org/10.1021/acsomega.3c05372
ACS Omega 2023, 8, 42632−42646

excited at their respective absorption maxima except **3d**, which has a prominent emission peak at 480 nm (Figure 5B).

Biological Activity. Preliminary studies showed that some Schiff bases **3** had antitumoral activity with a better therapeutic index (TI) than cisplatin, a standard chemotherapeutic drug, as well as activity against Gram-positive bacteria;[29] therefore, to expand the evaluation of the biological activity of synthesized compounds, anti-inflammatory and additional antimicrobial activities were evaluated.

Anti-inflammatory Activity. In order to assess the anti-inflammatory activity of Schiff base derivatives, RAW264.7 cells were pretreated with the compounds prior to stimulation with LPS, and the levels of NO in the culture media were determined by using the Griess method. The concentrations used were selected based on the IC_{50} values (Table S30), and cell viability at the end of the experiment was maintained at over 80% for all the controls and samples assayed (Figure 6). The activity of **3f** could not be determined due to the high inhibition of RAW264.7 proliferation observed.

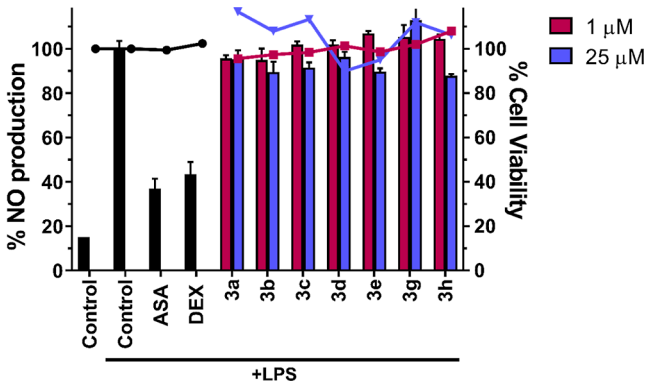

Figure 6. Anti-inflammatory activity of compounds **3a**−**3h**. RAW264.7 cells were pretreated with the derivatives and then stimulated with LPS. The percentage of NO production was calculated using cells treated with LPS only (control + LPS) as 100% NO production. Dexamethasone (DEX) and aspirin (ASA) were used as positive controls, and cells were only incubated with cell media as negative controls (control). Bars represent the percentage of the NO production. Lines represent the % cell viability for each corresponding set of data (black, controls; purple, 1 μM; and blue, 25 μM).

As shown in Figure 6, LPS stimulation resulted in a marked induction of NO production compared to that of untreated cells (control). The values obtained after the pretreatment with the derivatives alone without LPS stimulation were the same as those obtained with the negative control, only incubated with cell media (not shown).

Although pretreatment with 25 μM of **3b**, **3e**, and **3h** four h before LPS stimulation for 18 h reduced NO production compared to the control + LPS, the percentage of inhibition was lower when compared to the positive controls (dexamethasone and aspirin) (36.9 and 43.4% of NO production, respectively). The most effective of these three derivatives was **3h**, which reduced the NO production by 87.9%, followed by **3b** and **3e**. These results are consistent with other studies where the introduction of nitro groups in Schiff bases, such as in **3h**, presented higher anti-inflammatory activity compared to the presence of other groups.[41]

Antimicrobial Activity. On the other hand, to expand on the previously reported antibacterial activity of these compounds,[29] their activity was tested against many Gram-negative bacteria, including *Pseudomonas aeruginosa*, *Salmonella enterica*, *Klebsiella ozaenae*, and *Enterobacter gergoviae*. The minimum inhibitory concentrations (MICs) are shown in Table 4. MIC values above 250 μM were considered ineffective and labeled "non-active" (NA).

Table 4. MIC[a] and Type of Inhibition[b,c] Determined by Growth Kinetics over 20 h (OD_{600}) for Bacteria and over 72 h (OD_{530}) for Fungi after Serial Microdilution in 96-Well Plates for Active Schiff Bases

bacteria strain	3b	3f	3h
P. aeruginosa ATCC 27853	NA	NA	NA
S. enterica ATCC 14028	NA	31.25[c]	NA
K. ozaenae (clinical isolate)	NA	62.50[c]	NA
E. gergoviae (clinical isolate)	NA	15.60[b]	NA
Fungal Strain			
Candida albicans (clinical isolate)	250	15.60	125
Candida krusei (clinical isolate)	NA	62.50	NA
Candida tropicalis (clinical isolate)	NA	31.25	NA
Candida glabrata (clinical isolate)	NA	62.50	NA

[a]μM. [b]Bacteriostatic. [c]Bactericidal; NA: non-active.

We found that compounds **3a**, **3b**, **3c**, **3d**, **3e**, **3g**, and **3h** did not show antibacterial activities against the tested bacteria; however, Schiff base **3f** inhibited the bacterial growth of all strains, except *P. aeruginosa*, with the lowest MIC value (15.6 μM) against *E. gergoviae*. According to the observations, **3f** had a bactericidal effect on *S. enterica* and *K. ozaenae* while having a bacteriostatic effect on *E. gergoviae* (Table 4). Interestingly, none of the Schiff bases inhibited *P. aeruginosa* growth, which is consistent with previous findings;[16,42] however, it is unclear if the observed lack of activity is due to the Schiff base's structure, the mechanism of action, or both.

In addition to the tested bacterial strains, the antifungal activities were determined by testing the eight Schiff bases against clinical isolates of *Candida albicans*, *Candida krusei*, *Candida tropicalis*, and *Candida glabrata*. Compounds **3a**, **3b**, **3c**, **3d**, **3e**, and **3g** did not show any activity against the tested *Candida* strains; however, Schiff bases **3b**, **3f**, and **3h** showed fungal growth inhibition, and their MIC values are detailed in Table 4. MIC values above 250 μM were considered ineffective and labeled "NA".

Of the three compounds that showed antifungal activities, **3f** showed activity for all the tested strains (MIC < 100 μM), with the lowest MIC value of 15.6 μM for *C. albicans*. *C. albicans* was the only strain susceptible to three compounds (**3b**, **3f**, and **3h**). Interestingly, **3f** showed higher antifungal activity than **3h** and **3b** within the same strain, with MIC values at least 8 times lower.

Forming biofilms is widely accepted as an important factor in developing long-term infections and resistance to conventional antimicrobial therapy.[43] Studies have shown that biofilm communities are more resistant to antimicrobial treatments than planktonic cells,[44] highlighting the need for new compounds with antibiofilm potential. In this context, Schiff bases **3** were tested for their biofilm inhibitory ability against three biofilm-forming microorganisms: *Staphylococcus aureus*, *Enterococcus faecalis*, and *C. tropicalis*, and their MIC are shown in Table 5. MIC values above 250 μM were considered ineffective and labeled "NA".

Compounds **3a**, **3b**, **3c**, **3d**, and **3g** showed no biofilm inhibition activity against the tested microorganisms. On the other hand, compound **3f** inhibited biofilm formation in *S.*

https://doi.org/10.1021/acsomega.3c05372
ACS Omega 2023, 8, 42632−42646

Table 5. MIC[a] of Biofilm Inhibition Activity of Schiff Bases 3a−h against Biofilm-Forming Microorganisms at 24 h

bacteria strain	3e	3f	3h
S. aureus ATCC 25923	NA	62.50	NA
E. faecalis ATCC 29212	250	125	250
C. tropicalis (clinical isolate)	NA	62.50	250

[a]μM; NA: non-active.

aureus and *C. tropicalis* by 82.77 and 90.41%, respectively, at 62.5 μM, whereas *E. faecalis* inhibition was 75.69% at 125 μM. The other active compounds were **3h** and **3e**, which reduced biofilm formation in *E. faecalis* at a concentration of 250 μM by 76.63 and 69.05%, respectively. Finally, compound **3h** inhibited biofilm formation in *C. tropicalis* by 22.11% at the highest concentration evaluated.

As in the antibacterial evaluation, **3f** exhibited a remarkably high potential for biofilm inhibition. Bromide-containing compounds have been linked to this activity,[45,46] and several bromine-derived compounds have been reported to interfere with biofilm development through Quorum-sensing inhibition since these compounds can inactivate receptors involved in biofilm formation and other virulence factors.[47,48]

CONCLUSIONS

The Schiff-base derivatives **3a−h** can be readily synthesized with high yields by the condensation reaction between 4-AAP (**1**) and various cinnamaldehydes. Vibrational (IR), electronic (UV−vis), and fluorescence spectroscopy were used to characterize the structure. The theoretical results support assigning the vibrational and electronic spectra absorption bands. The crystal packing of **3b**, **3d**, **3g**, and **3h** showed intermolecular C−H···O and C−H···N hydrogen bonds, where 1*H*-pyrazole, benzene, methyl, and NO_2 moieties evidence important participation-generating intermolecular contacts that stabilize the supramolecular assembly by $R_3^3(24)$, $R_2^2(15)$, $R_2^2(16)$, $R_2^2(10)$, and $R_2^2(30)$ graph-set ring motifs. Moreover, the HS analysis revealed a dominant percentage of relative contributions C···H (range 21−26%) and H···H (range 41−61%) contacts due to the planarity of crystalline structures that generate $\pi\cdots\pi$ stacking, C−H···π, and C═O···π intermolecular interactions. Schiff-base derivative **3h** showed minor anti-inflammatory activity. Furthermore, Schiff bases **3f** and, to a lesser extent, **3h** and **3b**, have promising activity against a variety of clinically important bacteria and fungi and should be investigated further. The cytotoxicity observed in **3f** could be attributed to the bromine atom's oxidative properties, which favor microbial inhibition; nevertheless, more research is needed to understand this compound's actual mode of action.

EXPERIMENTAL SECTION

General Information. Dimethyl sulfoxide (DMSO, Fisher-certified reagent), molecular sieve 4 Å (Merck), all solvents, and other reagents were from Aldrich (St. Louis, MO, USA) and were used as received without further purification. All melting points were uncorrected and determined on a Fisher-Johns analogue melting point apparatus. FTIR spectra were recorded by a PerkinElmer FTIR Spectrum One using an ATR system (4000−650 cm^{-1}). The ^1H and ^{13}C NMR spectra were recorded at 298 K on a Bruker ADVANCE 500 MHz spectrometer equipped with a z-gradient, triple-resonance (^1H, ^{13}C, and ^{15}N) cryoprobe using DMSO-d_6 or $CDCl_3$ as solvents. Chemical shifts are expressed in ppm with TMS as an internal reference (TMS, δ = 0 ppm) for protons. Reactions were monitored by TLC on silica gel using ethyl acetate/hexane mixtures as a solvent and compounds visualized by a UV lamp. The reported yields are for the purified materials and are not optimized. Electrochemical experiments were carried out using a PGSTAT128N Autolab potentiostat (Metrohm AG), with Nova 2.1 software into a three-electrode cell composed of a graphite counter electrode (ca. 0.35 cm^2), a silver/silver chloride reference electrode (Ag/AgCl 3.0 M, CH Instruments), and a glassy carbon working electrode (3.0 mm diameter, CH Instruments). Voltammograms were obtained employing a scan rate of 100 mV/s into a 0.1 M solution of NMe_4ClO_4 with a concentration of ca. 1.0 mM of each target molecule. Before each measurement, argon was bubbled by ca. to 10 min to displace oxygen from the solution.

Synthesis of Schiff Bases 3a−h. All Schiff bases **3** were synthesized, as previously reported.[16,29] Equimolar amounts of 4-amino-1,5-dimethyl-2-phenylpyrazol-3-one (**1**) (1.722 mmol) and substituted cinnamaldehydes **2a−h** (1.722 mmol) were dissolved in 5.0 mL of EtOH and refluxed for 1 to 24 h, except for the synthesis of **3f**, which was carried out at room temperature. The progress of the reaction was monitored by TLC. After completion, the precipitates formed were filtered, washed, dried, and purified by recrystallization with ethanol. All compounds were characterized, and all of the data obtained agreed with the proposed structures (see Supporting Information).

X-ray Diffraction Data and Structural Solution and Refinement. The measurements were performed on an Oxford Xcalibur Gemini, Eos CCD diffractometer with graphite-monochromated MoKα (λ = 0.71073 Å) radiation. X-ray diffraction intensities were collected (ω scans with ϑ and κ-offsets), integrated, and scaled with the CrysAlisPro[49] suite of programs. The unit cell parameters were obtained by least-squares refinement (based on the angular setting for all collected reflections with intensities larger than seven times the standard deviation of measurement errors) using CrysAlisPro. The data were corrected empirically for absorption employing the multiscan method implemented in CrysAlisPro.

The non-H crystal structures of **3b**, **3d**, and **3h** were solved by the dual space procedure implemented in SHELXT[50] and the molecular model refined by full-matrix least-squares with SHELXL of the SHELX suite of programs.[51] At this stage, difference Fourier maps showed most hydrogen atoms. These, however, were positioned at their expected geometric locations and refined with the riding model. The methyl H-atoms were treated during the refinement as rigid groups allowed to rotate around the corresponding C−CH_3 or N−CH_3 bonds to maximize the sum of the residual electron density at the calculated H-positions.

Most of the diffraction pattern of the **3g** crystal was interpreted in terms of a two-component monoclinic twin. The unit cell parameters for both crystal domains were equal to experimental accuracy. These domains were rotated 180° from each other around the reciprocal c^* axis. The reflections were indexed in the reciprocal unit cell of the corresponding domains. It was resorted to the twin crystal data reduction facility implemented in CrysAlisPro to generate two datasets, namely, a regular one with the diffraction data indexed in the reciprocal unit cell of the largest domain (with about 57% diffracting power) and a second one including all reflections from both domains with the overlapping ones flagged for structure development and refinement. The first dataset was employed

https://doi.org/10.1021/acsomega.3c05372
ACS Omega 2023, 8, 42632−42646

to solve and refine the non-H structure as described above for the other compounds. Despite the correct molecular model, however, the refinement showed evidence for the presence of overlap between reflections from both crystal twins. This evidence included (besides the visual rendering of the weighted reciprocal space implemented in CrysAlisPro) a relatively high agreement R1-factor (0.192) and the most disagreeable reflections list showing systematically larger F(obs) as compared with F(calc) values. We therefore refined the initial molecular model against the second dataset, which includes all collected reflections for both crystal domains, employing the untwining process implemented in SHELXL. Now that the R1-factor has dropped to 0.077, the sign of F(obs) − F(calc) difference for the most disagreeable reflections was more evenly distributed, and a difference Fourier map showed all H-atoms. These, however, were positioned and refined with the riding model as detailed above.

Crystal data and structure refinement results are summarized in Tables S1 and S2. Crystallographic structural data have been deposited at the Cambridge Crystallographic Data Centre (CCDC). Any request to the CCDC for this material should quote the full literature citation and the reference numbers CCDC 2226611 (**3b**), 2226612 (**3d**), 2226613 (**3g**), and 2226614 (**3h**).

HS Calculations. The CrystalExplorer 17.5[52] program was used for the development of lattice energy and HS calculations. In this sense, the HS was evaluated by descriptors of surface, d_{norm} (normalized contact distance), shape index, and curvedness that decode and quantify intermolecular interactions in the crystal lattice. The d_{norm} surfaces were mapped over a fixed color scale of −0.078 au (red) − 0.657 au (blue). In addition, the shape index was mapped in the color range of −1.0 au (concave) − 1.0 au (convex) Å and curvedness in the range of −4.0 au (flat) − 0.4 au (singular) Å. The 2D-fingerprint plots (2D-FP) were used to visualize and decode the relative contributions of the main intermolecular contacts to the HS. Moreover, the intermolecular interaction energies were calculated using the TONTO program with the energy model CE-HF···HF/3-21G electron densities, integrated into the CrystalExplorer 17.5 program. The interaction energy and intermolecular contacts between molecules are expressed in terms of four components: electrostatic (E_{ele}), polarization (E_{pol}), dispersion (E_{dis}), and exchange-repulsion (E_{rep}). The 2D-FP were generated by using the translated (1.0−2.8 Å) range, and reciprocal contacts were included.

Electrochemical Characterization. Tetramethylammonium perchlorate (NMe_4ClO_4, ACS reagent, supporting electrolyte) and ferrocene (>98%) were acquired from Sigma-Aldrich. All reagents were employed as received without further purification processes. Electrochemical experiments were carried out using a PGSTAT128N Autolab potentiostat (Metrohm AG) with Nova 2.1 software in a three-electrode cell. The cell was composed of a graphite bar as a counter electrode (ca. 0.35 cm^2), a silver/silver chloride as a reference electrode (Ag/AgCl 3.0 M, CH Instruments, Inc.), and a glassy carbon as a working electrode (3.0 mm diameter, CH Instruments, Inc.). Voltammograms were obtained employing a scan rate of 100 mV/s into a 0.1 M solution of NMe_4ClO_4 in DMSO, with a concentration of ca. 1.0 mM of each target molecule. Before each measurement, argon was bubbled for approximately 10 min to displace oxygen from the solution.

Biological Evaluation. *Evaluation of Anti-inflammatory Activity.* RAW264.7 cells (1×10^5 cells/well) were seeded onto a 24−well culture plate and pretreated with 1, 25, and 50 μM of the compounds for 4 h. Dexamethasone (DEX) and aspirin (ASA) were used as controls. After, LPS (InvivoGen) at a final concentration of 1 μg/mL was added to the cells and incubated for an additional 18 h. NO production was monitored by adding 50 μL of Griess reagent (Sigma) to 50 μL of supernatants. After incubating for 10 min at room temperature in the dark, the absorbance was measured in a Cytation5 multimode detection system (BioTek) at 540 nm. The % reduction of NO was calculated using cells treated with LPS only as 100% NO production. Additionally, to assess cell viability after LPS stimulation, cells were washed with PBS and fixed with 4% paraformaldehyde for 20 min at room temperature before staining with 0.5% (w/v) crystal violet for 30 min at room temperature. Then, the plates were gently washed with water to eliminate the extra dye and left to dry at room temperature. Dried plates were scanned and quantified in a Cytation5 multimode detection system (BioTek) at 570 nm. Untreated cells were used as a 100% cell viability control.

Evaluation of Antibacterial Activity. The antibacterial activity of the eight Schiff bases was tested against the Gram-negative bacteria *P. aeruginosa* ATCC 27853, *S. enterica* ATCC 14028, *K. ozaenae*, and *E. gergoviae*, using the previously reported method.[29]

The bacterial inoculum, stock solutions, blanks, and controls were prepared as previously described.[29] Several antibiotics were used as controls for growth inhibition at the recommended working concentrations for the tested strains. Specifically, chloramphenicol (20 μg/mL) was used for *S. enterica* ATCC 14028 and *E. gergoviae*, tetracycline (10 μg/mL) was used for *K. ozaenae*, and streptomycin (100 μg/mL) was used for *P. aeruginosa* ATCC 27853.

Concentrations (0.5−250 μM) were used for the Schiff bases. The MIC was determined after tracking bacterial growth over 20 h in samples exposed to the tested compound at different concentrations. The MIC was defined as the lowest concentration of the antibacterial agent that completely inhibited the growth of the microorganism, as determined by the optical density at 600 nm. These assays were performed at least in triplicates.

Evaluation of Antifungal Activity. Antifungal activity was tested against the clinical isolates of *C. albicans* 13932, *C. krusei*, *C. glabrata*, and *C. tropicalis* using the microdilution method.[40,41,53]

The fungal inoculum was prepared in yeast dextrose peptone (YPD) media to a final cell density of 5×10^2 cells/mL. Stock solutions were prepared as described before. The final concentration of DMSO was 2.5% v/v, which was shown to not affect the fungal growth. As a control, fungal cells were grown with 2.5% DMSO to rule out any potential growth inhibitory effect. Additionally, nourseothricin was used as a control for growth inhibition at 200 μg/mL. YPD alone and that supplemented with the compounds at different concentrations were used as blanks.

Drug susceptibility was assessed with concentrations ranging between 15.6 and 250 μM. The following modifications were included: first, compounds were serially diluted in DMSO, then 5 μL of each dilution was added to 195 μL of fungal suspension (5×10^2 cells/mL) up to a total volume of 200 μL. The plates were then incubated at 35 °C for 72 h without shaking, and the OD_{530} was monitored every 30 min on a Cytation5 multimode detection system (BioTek). The MIC was determined after fungal growth was monitored for 72 h in samples exposed to the

https://doi.org/10.1021/acsomega.3c05372
ACS Omega 2023, 8, 42632−42646

tested compounds at different concentrations. These assays were performed at least in triplicate.

Evaluation of Biofilm Inhibition Activity. Bacterial strains: Gram-positive *S. aureus* ATCC 25923, *E. faecalis* ATCC 29212, and the fungal strain *C. tropicalis* (clinical isolate), were cultured in TSB + G (Tryptic Soy Broth medium supplemented with 1% Glucose) overnight.

1/100 dilution of the overnight culture was prepared, and aliquots of 150 μL were distributed into 96-well polystyrene microtiter plates along with a range of concentrations of Shiff bases **3a−h**. Plates were incubated under static conditions at 37 °C for 24 h.

The dilution stock solutions were prepared in 100% DMSO, and the final concentration of DMSO used in the assay was 2.5%. The minimum biofilm inhibitory concentration of the Shiff bases was determined by serial dilutions (250−15.62 μM). Concentrations were tested in technical duplicates during three independent biological replicates. All strains were also cultured with 2.5% DMSO (positive control) for the data analysis.

After a 24 h incubation period, the medium was carefully removed with a micropipette, and the plate was washed twice with PBS 1x (pH 7.2). The plate was dried inside a laboratory oven at 60 °C for 1 h. Subsequently, 150 μL of 0.1% crystal violet solution was added to each well for 20 min at room temperature. The staining solution was discarded, and wells were washed three times with 1x PBS (pH 7.2). Finally, 200 μL of 98% ethanol was added to each well, and the wells were incubated for 30 min at room temperature, and absorbance was measured at 590 nm. The biofilm inhibition percentage was calculated using the following formula

$$\text{inhibitory rate (\%)} = [OD_{590\,nm}\,(\text{positive control}) - OD_{590\,nm}\,(\text{sample}) / OD_{590\,nm}\,(\text{positive control})] \times 100$$

Computational Details. Quantum chemical calculations were performed for the ground state (gas phase) for **3a−h** with the program package Gaussian 09, Rev D.01. A conformational analysis around the free rotation bond C7−C8−N3−C12 (see Figures 1 and S39) was performed with the semiempirical method PM6/ZDO to explore minimum energy conformations. To confirm the stability of the optimized conformations, vibrational frequency calculations were performed at the same level of theory (PM6/ZDO). No scaling factor was applied to the computed frequencies. In all cases, the energy minima structures have no imaginary values of frequencies. The electronic transitions were calculated with the time-dependent density functional theory at the same theory level without the solvent's implicit effect.

■ ASSOCIATED CONTENT

Supporting Information

The Supporting Information is available free of charge at https://pubs.acs.org/doi/10.1021/acsomega.3c05372.

Copies of ^{1}H NMR and IR spectra from synthesized compounds; crystallographic data, HSs, and intermolecular interactions of compounds **3b**, **3d**, **3g**, and **3h**; molecular orbitals involved in the electronic transitions; potential energy curves of all Schiff bases; and cytotoxicity of all synthesized compounds on RAW264.7 cells (PDF)

■ AUTHOR INFORMATION

Corresponding Author

Jorge Heredia-Moya − *Centro de Investigación Biomédica (CENBIO), Facultad de Ciencias de la Salud Eugenio Espejo, Universidad UTE, Quito 170527, Ecuador;* orcid.org/0000-0001-7620-9140; Phone: +593-2-2990800 (ext. 2538); Email: jorgeh.heredia@ute.edu.ec

Authors

Esteban Aguilar-Llanos − *Facultad de Ciencias Químicas, Universidad Central del Ecuador, Francisco Viteri s/n y Gilberto Gato Sobral, Quito 170521, Ecuador*

Saskya E. Carrera-Pacheco − *Centro de Investigación Biomédica (CENBIO), Facultad de Ciencias de la Salud Eugenio Espejo, Universidad UTE, Quito 170527, Ecuador*

Rebeca González-Pastor − *Centro de Investigación Biomédica (CENBIO), Facultad de Ciencias de la Salud Eugenio Espejo, Universidad UTE, Quito 170527, Ecuador*

Johana Zúñiga-Miranda − *Centro de Investigación Biomédica (CENBIO), Facultad de Ciencias de la Salud Eugenio Espejo, Universidad UTE, Quito 170527, Ecuador*

Cristina Rodríguez-Pólit − *Centro de Investigación Biomédica (CENBIO), Facultad de Ciencias de la Salud Eugenio Espejo, Universidad UTE, Quito 170527, Ecuador*

Arianna Mayorga-Ramos − *Centro de Investigación Biomédica (CENBIO), Facultad de Ciencias de la Salud Eugenio Espejo, Universidad UTE, Quito 170527, Ecuador;* orcid.org/0000-0003-0220-4990

Oscar Carrillo-Naranjo − *Centro de Investigación Biomédica (CENBIO), Facultad de Ciencias de la Salud Eugenio Espejo, Universidad UTE, Quito 170527, Ecuador*

Linda P. Guamán − *Centro de Investigación Biomédica (CENBIO), Facultad de Ciencias de la Salud Eugenio Espejo, Universidad UTE, Quito 170527, Ecuador*

Juan Carlos Romero-Benavides − *Departamento de Química, Facultad de Ciencias Exactas y Naturales, Universidad Técnica Particular de Loja, Loja 1101608, Ecuador*

Carlos Cevallos-Morillo − *Facultad de Ciencias Químicas, Universidad Central del Ecuador, Francisco Viteri s/n y Gilberto Gato Sobral, Quito 170521, Ecuador;* Present Address: Facultad de Medicina, Universidad de las Américas, Quito, Ecuador

Gustavo A. Echeverría − *Departamento de Física, Facultad de Ciencias Exactas, Universidad Nacional de La Plata and Institute IFLP (CONICET, CCT-La Plata), C. C. 67, La Plata 1900, Argentina*

Oscar E. Piro − *Departamento de Física, Facultad de Ciencias Exactas, Universidad Nacional de La Plata and Institute IFLP (CONICET, CCT-La Plata), C. C. 67, La Plata 1900, Argentina*

Christian D. Alcívar-León − *Facultad de Ciencias Químicas, Universidad Central del Ecuador, Francisco Viteri s/n y Gilberto Gato Sobral, Quito 170521, Ecuador*

Complete contact information is available at: https://pubs.acs.org/10.1021/acsomega.3c05372

Notes

The authors declare no competing financial interest.

■ ACKNOWLEDGMENTS

We thank CONICET (grant PIP 0651) and UNLP (grant 11/X857) of Argentina for their financial support. G.A.E. and O.E.P.

are Research Fellows of CONICET. We would like to thank the Instituto de Microbiologia de la Universidad San Francisco de Quito for providing some ATCC bacteria used in this study.

REFERENCES

(1) Deshmukh, P.; Soni, P. K.; Kankoriya, A.; Halve, A. K.; Dixit, R. 4-Aminoantipyrine: A Significant Tool for the Synthesis of Biologically Active Schiff Bases and Metal Complexes. *Int. J. Pharm. Sci. Rev. Res.* **2015**, *34* (1), 162−170.
(2) Catalano, A.; Sinicropi, M. S.; Iacopetta, D.; Ceramella, J.; Mariconda, A.; Rosano, C.; Scali, E.; Saturnino, C.; Longo, P. A Review on the Advancements in the Field of Metal Complexes with Schiff Bases as Antiproliferative Agents. *Appl. Sci.* **2021**, *11* (13), 6027.
(3) Matela, G. Schiff Bases and Complexes: A Review on Anti-Cancer Activity. *Anticancer. Agents Med. Chem.* **2020**, *20* (16), 1908−1917.
(4) Sakthivel, A.; Jeyasubramanian, K.; Thangagiri, B.; Raja, J. D. Recent Advances in Schiff Base Metal Complexes Derived from 4-Aminoantipyrine Derivatives and Their Potential Applications. *J. Mol. Struct.* **2020**, *1222*, 128885.
(5) Zhang, J.; Xu, L.; Wong, W. Y. Energy Materials Based on Metal Schiff Base Complexes. *Coord. Chem. Rev.* **2018**, *355*, 180−198.
(6) Arumugam, A.; Shanmugam, R.; Munusamy, S.; Muhammad, S.; Algarni, H.; Sekar, M. Study of the Crystal Architecture, Optoelectronic Characteristics, and Nonlinear Optical Properties of 4-Amino Antipyrine Schiff Bases. *ACS Omega* **2023**, *8*, 15168−15180.
(7) Nibila, T. A.; Ahamed, T. S.; Soufeena, P. P.; Muraleedharan, K.; Periyat, P.; Aravindakshan, K. K. Synthesis, Structural Characterization, Hirshfeld Surface and DFT Based Reactivity, UV Filter and NLO Studies of Schiff Base Analogue of 4-Aminoantipyrine. *Results Chem.* **2020**, *2*, 100062.
(8) Ebosie, N. P.; Ogwuegbu, M. O. C.; Onyedika, G. O.; Onwumere, F. C. Biological and Analytical Applications of Schiff Base Metal Complexes Derived from Salicylidene-4-Aminoantipyrine and Its Derivatives: A Review. *J. Iran. Chem. Soc.* **2021**, *18* (12), 3145−3175.
(9) Kumari, N.; Singh, S.; Baral, M.; Kanungo, B. K. Schiff Bases: A Versatile Fluorescence Probe in Sensing Cations. *J. Fluoresc.* **2023**, *33* (3), 859−893.
(10) Ismail, A. H.; Al-Zaidi, B. H.; Abd, A. N.; Habubi, N. F. Synthesis and Characterization of Novel Thin Films Derived from Pyrazole-3-One and Its Metal Complex with Bivalent Nickel Ion to Improve Solar Cell Efficiency. *Chem. Pap.* **2020**, *74* (7), 2069−2078.
(11) Bhat, A. P. I.; Inam, F.; Bhat, B. R. Nickel Catalyzed One Pot Synthesis of Biaryls under Air at Room Temperature. *RSC Adv.* **2013**, *3* (44), 22191.
(12) Okey, N. C.; Obasi, N. L.; Ejikeme, P. M.; Ndinteh, D. T.; Ramasami, P.; Sherif, E.-S. M.; Akpan, E. D.; Ebenso, E. E. Evaluation of Some Amino Benzoic Acid and 4-Aminoantipyrine Derived Schiff Bases as Corrosion Inhibitors for Mild Steel in Acidic Medium: Synthesis, Experimental and Computational Studies. *J. Mol. Liq.* **2020**, *315*, 113773.
(13) Raczuk, E.; Dmochowska, B.; Samaszko-Fiertek, J.; Madaj, J. Different Schiff Bases—Structure, Importance and Classification. *Molecules* **2022**, *27* (3), 787.
(14) Ceramella, J.; Iacopetta, D.; Catalano, A.; Cirillo, F.; Lappano, R.; Sinicropi, M. S. A Review on the Antimicrobial Activity of Schiff Bases: Data Collection and Recent Studies. *Antibiotics* **2022**, *11* (2), 191.
(15) Kasare, M. S.; Dhavan, P. P.; Shaikh, A. H. I.; Jadhav, B. L.; Pawar, S. D. Novel Schiff Base Scaffolds Derived from 4-aminoantipyrine and 2-hydroxy-3-methoxy-5-(Phenyldiazenyl)Benzaldehyde: Synthesis, Antibacterial, Antioxidant and Anti-inflammatory. *J. Mol. Recognit.* **2022**, *35* (9), No. e2976.
(16) Teran, R.; Guevara, R.; Mora, J.; Dobronski, L.; Barreiro-Costa, O.; Beske, T.; Pérez-Barrera, J.; Araya-Maturana, R.; Rojas-Silva, P.; Poveda, A.; Heredia-Moya, J. Characterization of Antimicrobial, Antioxidant, and Leishmanicidal Activities of Schiff Base Derivatives of 4-Aminoantipyrine. *Molecules* **2019**, *24* (15), 2696.
(17) Çakmak, R.; Başaran, E.; Boğa, M.; Erdoğan, O.··.; Çınar, E.; Çevik, Ö. Schiff Base Derivatives of 4-Aminoantipyrine as Promising Molecules: Synthesis, Structural Characterization, and Biological Activities. *Russ. J. Bioorganic Chem.* **2022**, *48* (2), 334−344.
(18) Çakmak, R.; Başaran, E.; Şentürk, M. Synthesis, Characterization, and Biological Evaluation of Some Novel Schiff Bases as Potential Metabolic Enzyme Inhibitors. *Arch. Pharm. (Weinheim).* **2022**, *355* (4), 2100430.
(19) Kobzar, O. L.; Tatarchuk, A. V.; Kachaeva, M. V.; Pilyo, S. G.; Sukhoveev, O. V.; Sukhoveev, V. V.; Brovarets, V. S.; Vovk, A. I. Azomethine Derivatives of P-Aminobenzoic Acid as Antioxidants and Xanthine Oxidase Inhibitors. *Reports Natl. Acad. Sci. Ukr.* **2020**, No. 6, 74−82.
(20) Mermer, A.; Demirbas, N.; Uslu, H.; Demirbas, A.; Ceylan, S.; Sirin, Y. Synthesis of Novel Schiff Bases Using Green Chemistry Techniques; Antimicrobial, Antioxidant, Antiurease Activity Screening and Molecular Docking Studies. *J. Mol. Struct.* **2019**, *1181*, 412−422.
(21) Erturk, A. G. Synthesis, Structural Identifications of Bioactive Two Novel Schiff Bases. *J. Mol. Struct.* **2020**, *1202*, 127299.
(22) Baluja, S.; Chanda, S. Synthesis, Characterization and Antibacterial Screening of Some Schiff Bases Derived from Pyrazole and 4-Amino Antipyrine. *Rev. Colomb. Ciencias Químico-Farmacéuticas* **2016**, *45* (2), 201.
(23) Anupama, B.; Aruna, A.; Manga, V.; Sivan, S.; Sagar, M. V.; Chandrashekar, R. Synthesis, Spectral Characterization, DNA/ Protein Binding, DNA Cleavage, Cytotoxicity, Antioxidative and Molecular Docking Studies of Cu(II)Complexes Containing Schiff Base-Bpy/ Phen Ligands. *J. Fluoresc.* **2017**, *27* (3), 953−965.
(24) Gowda, J. I.; Nandibewoor, S. T. Binding and Conformational Changes of Human Serum Albumin upon Interaction with 4-Aminoantipyrine Studied by Spectroscopic Methods and Cyclic Voltammetry. *Spectrochim. Acta Mol. Biomol. Spectrosc.* **2014**, *124*, 397−403.
(25) Shanuja, K.; Pandiyan, R. P.; Arun, T.; Raman, N.; Shanuja, S. K.; Gnanamani, A. Preliminary Investigation of DNA Interaction and Antimicrobial Efficacy of 4-Amino-2,3-Dimethyl-1-Phenyl-3-Pyrazolin-5-One Incorporated Metal Complexes. *Int. J. Inorg. Bioinorg. Chem.* **2016**, *6* (1), 23−34.
(26) Paulpandiyan, R.; Raman, N. DNA Binding Propensity and Nuclease Efficacy of Biosensitive Schiff Base Complexes Containing Pyrazolone Moiety: Synthesis and Characterization. *J. Mol. Struct.* **2016**, *1125*, 374−382.
(27) Ani, F. E.; Ibeji, C. U.; Obasi, N. L.; Kelani, M. T.; Ukogu, K.; Tolufashe, G. F.; Ogundare, S. A.; Oyeneyin, O. E.; Maguire, G. E. M.; Kruger, H. G. Crystal, Spectroscopic and Quantum Mechanics Studies of Schiff Bases Derived from 4-Nitrocinnamaldehyde. *Sci. Rep.* **2021**, *11* (1), 8151.
(28) Arroudj, S.; Bouchouit, M.; Bouchouit, K.; Bouraiou, A.; Messaadia, L.; Kulyk, B.; Figa, V.; Bouacida, S.; Sofiani, Z.; Taboukhat, S. Synthesis, Spectral, Optical Properties and Theoretical Calculations on Schiff Bases Ligands Containing o-Tolidine. *Opt. Mater. (Amst).* **2016**, *56*, 116−120.
(29) Aguilar-Llanos, E.; Carrera-Pacheco, S. E.; González-Pastor, R.; Zúñiga-Miranda, J.; Rodríguez-Pólit, C.; Romero-Benavides, J. C.; Heredia-Moya, J. Synthesis and Evaluation of Biological Activities of Schiff Base Derivatives of 4-Aminoantipyrine and Cinnamaldehydes. *Chem. Proc.* **2022**, *12* (1), 43.
(30) Li, Y.; Liu, Y.; Wang, H.; Xiong, X.; Wei, P.; Li, F. Synthesis, Crystal Structure, Vibration Spectral, and DFT Studies of 4-Aminoantipyrine and Its Derivatives. *Molecules* **2013**, *18* (1), 877−893.
(31) Farrugia, L. J. WinGX and ORTEP for Windows : An Update. *J. Appl. Crystallogr.* **2012**, *45* (4), 849−854.
(32) Elgrishi, N.; Rountree, K. J.; McCarthy, B. D.; Rountree, E. S.; Eisenhart, T. T.; Dempsey, J. L. A Practical Beginner's Guide to Cyclic Voltammetry. *J. Chem. Educ.* **2018**, *95* (2), 197−206.
(33) Sandford, C.; Edwards, M. A.; Klunder, K. J.; Hickey, D. P.; Li, M.; Barman, K.; Sigman, M. S.; White, H. S.; Minteer, S. D. A Synthetic Chemist's Guide to Electroanalytical Tools for Studying Reaction Mechanisms. *Chem. Sci.* **2019**, *10* (26), 6404−6422.
(34) Gowda, J. I.; Nandibewoor, S. T. Electrochemical Behavior of 4-Aminophenazone Drug at a Graphite Pencil Electrode and Its

https://doi.org/10.1021/acsomega.3c05372
ACS Omega 2023, 8, 42632−42646

Application in Real Samples. *Ind. Eng. Chem. Res.* **2012**, *51* (49), 15936−15941.
(35) Hamurcu, F.; Mamaş, S.; Ozdemir, U. O.; Gündüzalp, A. B.; Senturk, O. S. New Series of Aromatic/ Five-Membered Heteroaromatic Butanesulfonyl Hydrazones as Potent Biological Agents: Synthesis, Physicochemical and Electronic Properties. *J. Mol. Struct.* **2016**, *1118*, 18−27.
(36) Andres, T.; Eckmann, L.; Smith, D. K. Voltammetry of Nitrobenzene with Cysteine and Other Acids in DMSO. Implications for the Biological Reactivity of Reduced Nitroaromatics with Thiols. *Electrochim. Acta* **2013**, *92*, 257−268.
(37) Obasi, L. N.; Kaior, G. U.; Rhyman, L.; Alswaidan, I. A.; Fun, H.-K.; Ramasami, P. Synthesis, Characterization, Antimicrobial Screening and Computational Studies of 4-[3-(4-Methoxy-Phenyl)-Allylideneamino]-1,5-Dimethyl-2-Phenyl-1,2-Dihydro-Pyrazol-3-One. *J. Mol. Struct.* **2016**, *1120*, 180−186.
(38) Guimarães, C.; Bento, R. R. F.; Faria, J. L. B.; Ramos, R. J.; Silva, L. E.; Freire, P. T. C.; Gusmão, G.; Teixeira, A. M. R. Vibrational Spectra of (4E)-4-((E)-3-Phenyl-Allylideneamino)-1,2-Dihydro-2,3-Dimethyl-1-Phenylpirazol-5-One. *J. Mol. Struct.* **2011**, *1006* (1−3), 589−595.
(39) Eltayeb, N. E.; Şen, F.; Lasri, J.; Hussien, M. A.; Elsilk, S. E.; Babgi, B. A.; Gökce, H.; Sert, Y. Hirshfeld Surface Analysis, Spectroscopic, Biological Studies and Molecular Docking of (4E)-4-((Naphthalen-2-Yl)Methyleneamino)-1,2-Dihydro-2,3-Dimethyl-1-Phenylpyrazol-5-One. *J. Mol. Struct.* **2020**, *1202* (xxxx), 127315.
(40) El-Nahass, M. M.; Kamel, M. A.; El-Menyawy, E. M. Spectroscopic Analysis of 2-(2,3-Dihydro-1,5-Dimethyl-3-Oxo-2-Phenyl-1H-Pyrazol-4-Ylimino)-2-(4-Nitro-Phenyl) Acetonitrile. *Spectrochim. Acta Part A Mol. Biomol. Spectrosc.* **2011**, *79* (3), 618−624.
(41) Roriz, B. C.; Buccini, D. F.; Dos Santos, B. F.; Silva, S. R. d. S.; Domingues, N. L. d. C.; Moreno, S. E. Synthesis and Biological Activities of a Nitro-Shiff Base Compound as a Potential Anti-Inflammatory Agent. *Eur. J. Pharm. Sci.* **2020**, *148*, 105300.
(42) Aguzue, O. C.; Adedayo, A.; Phillip, O. A. Mechanochemical Synthesis and Potentiation of the Antimicrobial Activity of 4-[3-(4-Methoxyphenyl)-Allylideneamino]-1,5-Dimethyl-2-Phenylpyrazol-3-One by Metal Chelation. *J. Sci. Math. Lett.* **2020**, *8* (2), 15−21.
(43) Römling, U.; Balsalobre, C. Biofilm Infections, Their Resilience to Therapy and Innovative Treatment Strategies. *J. Int. Med.* **2012**, *272* (6), 541−561.
(44) Olsen, I. Biofilm-Specific Antibiotic Tolerance and Resistance. *Eur. J. Clin. Microbiol. Infect. Dis.* **2015**, *34* (5), 877−886.
(45) de Lima Pimenta, A.; Chiaradia-Delatorre, L. D.; Mascarello, A.; de Oliveira, K. A.; Leal, P. C.; Yunes, R. A.; de Aguiar, C. B. N. M.; Tasca, C. I.; Nunes, R. J.; Smânia, A. Synthetic Organic Compounds with Potential for Bacterial Biofilm Inhibition, a Path for the Identification of Compounds Interfering with Quorum Sensing. *Int. J. Antimicrob. Agents* **2013**, *42* (6), 519−523.
(46) Pandolfi, F.; D'Acierno, F.; Bortolami, M.; De Vita, D.; Gallo, F.; De Meo, A.; Di Santo, R.; Costi, R.; Simonetti, G.; Scipione, L. Searching for New Agents Active against Candida Albicans Biofilm: A Series of Indole Derivatives, Design, Synthesis and Biological Evaluation. *Eur. J. Med. Chem.* **2019**, *165*, 93−106.
(47) Park, J. S.; Ryu, E.-J.; Li, L.; Choi, B.-K.; Kim, B. M. New Bicyclic Brominated Furanones as Potent Autoinducer-2 Quorum-Sensing Inhibitors against Bacterial Biofilm Formation. *Eur. J. Med. Chem.* **2017**, *137*, 76−87.
(48) Vashistha, A.; Sharma, N.; Nanaji, Y.; Kumar, D.; Singh, G.; Barnwal, R. P.; Yadav, A. K. Quorum Sensing Inhibitors as Therapeutics: Bacterial Biofilm Inhibition. *Bioorg. Chem.* **2023**, *136*, 106551.
(49) *CrysAlisPro Software System*; Rigaku Corporation: Oxford, UK, 2015.
(50) Sheldrick, G. M. SHELXT - Integrated Space-Group and Crystal-Structure Determination. *Acta Crystallogr. Sect. A Found. Adv.* **2015**, *71* (1), 3−8.
(51) Sheldrick, G. M. A Short History of SHELX. *Acta Crystallogr. Sect. A Found. Crystallogr.* **2008**, *64* (1), 112−122.
(52) Spackman, P. R.; Turner, M. J.; Mckinnon, J. J.; Wolff, S. K.; Grimwood, D. J.; Jayatilaka, D.; Spackman, M. A. *CrystalExplorer*: a program for Hirshfeld surface analysis, visualization and quantitative analysis of molecular crystals. *J. Appl. Crystallogr.* **2021**, *54*, 1006−1011.
(53) Balouiri, M.; Sadiki, M.; Ibnsouda, S. K. Methods for in Vitro Evaluating Antimicrobial Activity: A Review. *J. Pharm. Anal.* **2016**, *6* (2), 71−79.

https://doi.org/10.1021/acsomega.3c05372
ACS Omega 2023, 8, 42632−42646